University of North Dakota
UND Scholarly Commons

Theses and Dissertations
Theses, Dissertations, and Senior Projects

January 2022

Energy Harvesting & Wing Morphing Design Using Piezoelectric Macro Fiber Composites

Md Saifuddin Ahmed Atique

How does access to this work benefit you? Let us know!

Follow this and additional works at: https://commons.und.edu/theses

Recommended Citation

Atique, Md Saifuddin Ahmed, "Energy Harvesting & Wing Morphing Design Using Piezoelectric Macro Fiber Composites" (2022). *Theses and Dissertations*. 4251.
https://commons.und.edu/theses/4251

This Thesis is brought to you for free and open access by the Theses, Dissertations, and Senior Projects at UND Scholarly Commons. It has been accepted for inclusion in Theses and Dissertations by an authorized administrator of UND Scholarly Commons. For more information, please contact und.commons@library.und.edu.

ENERGY HARVESTING & WING MORPHING DESIGN USING PIEZOELECTRIC MACRO FIBER COMPOSITES

by

Md Saifuddin Ahmed Atique

Bachelor of Science, Military Institute of Science & Technology, 2016

A Thesis

Submitted to the Graduate Faculty

of the

University of North Dakota

in partial fulfillment of the requirements

for the degree of

Master of Science (M.Sc.)
Mechanical Engineering

Grand Forks, North Dakota

May

2022

Copyright 2022 Md Saifuddin Ahmed Atique

Name: Md Saifuddin Ahmed Atique

Degree: Master of Science

This document, submitted in partial fulfillment of the requirements for the degree from the University of North Dakota, has been read by the Faculty Advisory Committee under whom the work has been done and is hereby approved.

DocuSigned by:
Cai Xia Yang
9981400CA3EC436...
Dr. Cai Xia Yang

DocuSigned by:
Iraj Mamaghani
76231706E0AA4C6...
Dr. Iraj H.P Mamaghani

DocuSigned by:
Olusegun Stanley Tomomewo
894BC27CC43F4AB...
Dr. Olusegun Stanley Tomomewo

This document is being submitted by the appointed advisory committee as having met all the requirements of the School of Graduate Studies at the University of North Dakota and is hereby approved.

DocuSigned by:
Chris Nelson
2E6AF000C733409...
Chris Nelson
Dean of the School of Graduate Studies

3/3/2022
Date

PERMISSION

Title:	Energy Harvesting & Wing Morphing Design Using Piezoelectric Macro Fiber Composites
Department:	Mechanical Engineering
Degree:	Master of Science (M.Sc.)

In presenting this dissertation in partial fulfillment of the requirements for a graduate degree from the University of North Dakota, I agree that the library of this University shall make it freely available for inspection. I further agree that permission for extensive copying for scholarly purposes may be granted by the professor who supervised my dissertation work or, in his absence, by the Chairperson of the department or the dean of the Graduate School. It is understood that any copying or publication or other use of this dissertation or part thereof for financial gain shall not be allowed without my written permission. It is also understood that due recognition shall be given to me and to the University of North Dakota in any scholarly use which may be made of any material in my dissertation.

Md Saifuddin Ahmed Atique
February 2022

TABLE OF CONTENTS

LIST OF FIGURES

LIST OF TABLES

NOMENCLATURE

c = chord length

C_D = drag coefficient

C_L = lift coefficient

Re_c = Reynolds number based on the chord

s = model span (width)

U = flow velocity

x = streamwise coordinate

y = spanwise coordinate

z = normal coordinate

α = angle of attack of the airfoil

ω_y = vorticity along y

∞ = freestream conditions

C_M = pitching-moment coefficient about c/4

D = drag force

L = lift force

l = local coordinate tangent to the airfoil surface

n = local coordinate normal to the airfoil surface

s = model span (from wall to wall of the wind tunnel)

ξ= axial (chordwise) coordinate of the airfoil

ζ = normal coordinate of the airfoil

c_p = center of pressure

T=Bending Stress Component

S= Bending Stress Component

Y= Young's modulus

D_3= electric displacement component

S_3= Strain Component

E_3= e electric field component

$\bar{e}_{33}$= effective piezoelectric constant,

$\bar{C}^{E}_{33}$= effective elastic stiffness component (Young's modulus) at constant electric filed

M (x,t)= internal bending moment

W(x,t)= transverse deflection relative to the fixed frame

C_sI= strain-rate

C_a= viscous air damping coefficient

m= mass per unit length of the beam

g(t)= base translation in the transverse direction

$h(t)$= superimposed small rotation of the base

YI= Bending Stiffness

$\Gamma(x)$= spatial distribution of the electric potential

N_e= number of electrodes

u_e= width of each electrode

u_0= width of each non-electrode

$H(x)$= Heaviside function

B_{pt}= total width of the piezoelectric fibers

h_p= thickness of the piezoelectric fibers

h_d= position of top piezoceramic fiber

$\mathbf{D}$ = electric displacement vector

b_{act}= width of the active region

b_{ep}= width of epoxy fiber

N_p= number of piezoceramic fiber

Δ_{el}= effective electrode spacing

h_{ka}= thickness of Kapton layer (active region)

h_{ki}= thickness of Kapton layer (inactive region)

ACKNOWLEDGMENTS

At first, I express my deepest gratitude to my academic and research advisor Dr. Cai Xia Yang for her caring guidance and help throughout my research and for gladly offering me her knowledge and experience when needed. I really appreciate her way of thinking and always very welcoming positive will to except any new ideas/concepts and her extraordinary human being qualities. Thanks for making my journey at UND and Grand Forks so nice and memorable. Her trust and support were extremely encouraging and helpful.

I would also like to express my special thanks and highest appreciation to my M.Sc. committee; Dr. Iraj H.P. Mamaghani & Dr. Olusegun Tomomewo for their support and help. Additionally, I would like to express my appreciation to University of North Dakota for allowing me to do research and giving me opportunities to participate in various conferences held in the USA. I am thankful for the support from the University of North Dakota during the COVID-19 pandemic time. Also, I would like to thank my friends and colleagues from Mechanical Engineering Department.

I am ever thankful to my family members. I couldn't but remember my parents Mohammad Jalal Ahmmed and Khodeza Akter Baby. Though I was thousands of miles away from them, my home country Bangladesh and on the other side of the Atlantic Ocean, they have always been presented to love and support me under any circumstances. Last, but not least, I wouldn't be able to reach here today without all the unconditional love, care, and encouragement from my wife Samia Afrin. You are the best thing ever happened in my life. I am so blessed to have you.

To my parents

ABSTRACT

Energy harvesting from vibration sources was a very promising field of research throughout the last few decades among the engineers and scientist as considering the necessity of renewable/green energy for the welfare of mankind. Unused vibration energy exists in the surrounding or machineries was always tried to be utilized. Since then, by using piezoelectric transduction, researchers started to harvest the vibration energy. However, after the invention of piezo ceramics Macro Fiber Composites (MFC) by NASA, the research in this field augmented a lot due to its high efficiency to convert mechanical strain or vibration to useful electrical power and vice versa. Apart from energy harvesting researcher concentrated to utilize this harvested energy for daily life and hence application of this harvested energy for structural health monitoring inaugurated. Recent study showed that, the vibration energy harvested from the vehicles or aerospace (UAV) structure is good enough to power its onboard structural health monitoring unit though for feeding this power to any other onboard electrical system is still challenging due to low power generation along with its random production. Moreover, Macro Fiber Composites (MFC) can be used as an actuator to change the shape of aircraft wing to enhance aerodynamic performance and hence, application of MFC for wing morphing design has become popular throughout these years. The purpose of this research work is to depict the recent progress & development that took place in the field of energy harvesting & wing morphing research using macro fiber composites and combining the existing knowledge continue the work further, the future of this harvested energy, new design concept & upcoming challenges along with its possible solution. This work investigates the different configuration of macro fiber composites (MFC) for piezoelectric energy harvesting and its contribution for wing morphing design with enhanced aerodynamics. For the first part of this work, uniform MFC configuration was modeled and built up based on the Euler-Bernoulli beam theory. When the governing differential equations of the systems were derived, by applying the harmonic base excitation, coupled vibration response and the voltage response were obtained. The prediction of the mathematical model was at first verified by unimorph MFC with a brass substrate obtained from the state of art and then validation was justified by MFC unimorph along with three different substrate materials (copper, zinc alloy & galvanized steel) and thickness for the first time in this type of research. Computational & analytical solution revealed that, among these three substrates and for same thickness, maximum peak power at resonance excitation was obtained for the copper substrate. For the second part of the study (i) computational analysis was performed and the output was compared with the real time data obtained from the wind tunnel experiment and the conclusion stood that, with the increment of the incoming flow velocity, the power output from the MFC increases with a thin aerofoil made of copper substrates and two MFC on its upper surface (ii) wing morphing design was performed for a NACA 0012 aerofoil for the first time where macro fiber composite actuators were used to change the top and bottom surfaces of the aerofoil with a view to recording the enhanced aerodynamics performance the designed morphing wing. CFD simulation results were compared with the wind tunnel testing data from the state of art for NACA 0014 for all identical parameters. The enhanced aerodynamics performance observed for designed wing morphing can be used for future concepts like maneuvering of the aircraft without the help of ailerons or for the purpose of active flow control over the aircraft wing.

CHAPTER 1

INTRODUCTION

1.1 Fundamentals of Piezoelectric Energy Harvesting

A material has piezoelectric properties if it could transform mechanical strain energy into electrical energy and electrical energy into mechanical strain. Piezoelectric materials are from ferroelectric's materials. One of the unique sides of ferroelectric material is that this type of material exhibits local charge separation. Local charge separation is an electric dipole in the engineering field. However, for the ferroelectric materials, usually, these electric dipoles are oriented randomly throughout the material. They get reoriented while heating the material above a cruise temperature point and when a strong electric field is applied.

Dipoles orient themselves relative to the applied electric field. Once the material becomes cooled, the dipoles remain in the same orientation— then poling happens**.** After completing these jobs, the prepared material will exhibit the piezoelectric effect. The most efficient and productive way of harvesting energy from piezoelectric material is to use mechanical vibration. Mechanical vibration causes strain or the piezoelectric material, which provides a flow of electrons that power electrical devices. In 1996, Williams and Yates designed a device that could scavenge energy from the surrounding vibration source and produce electrical energy. However, to evaluate and optimize the viability of the energy harvester, harmonic analysis was performed— which determined that the total amount of energy harvested was proportional to the cube of the vibration frequency. They concluded that the amount of harvested energy is poor at low frequencies. A low damping factor is required to achieve the optimum harvested energy. According to their experiment, for maximizing harvested energy/power, a large amount of deflection in the structure was recommended.

1.2 Piezoelectric Materials

Piezoelectric materials refer to those that can produce electricity while placed under mechanical stress. They can generate an electric current while a mechanical strain is applied. At the same time, they can show the opposite**,** like when the input is an electric current, they can change their shape. These unusual properties offered by a few dielectric materials or the nature they show are known as piezoelectricity. Piezoelectric materials can have two kinds: polar and non-polar.

1.3 Piezoelectric Effect

Pierre and Jacques Curie first observed the piezoelectric effect. With the help of their knowledge of pyroelectricity, crystal structure, and behavior**,** they demonstrated the first piezoelectric effect by quartz, topaz, cane sugar and Rochelle salt. Nowadays, many electronic devices, especially the voice recognition one, i.e., Siri and even the microphone, use piezoelectricity. The piezoelectric crystal receives the sound energy from our voice and converts it. There are two types of piezoelectric effects: the direct piezoelectric effect and the inverse piezoelectric effect.

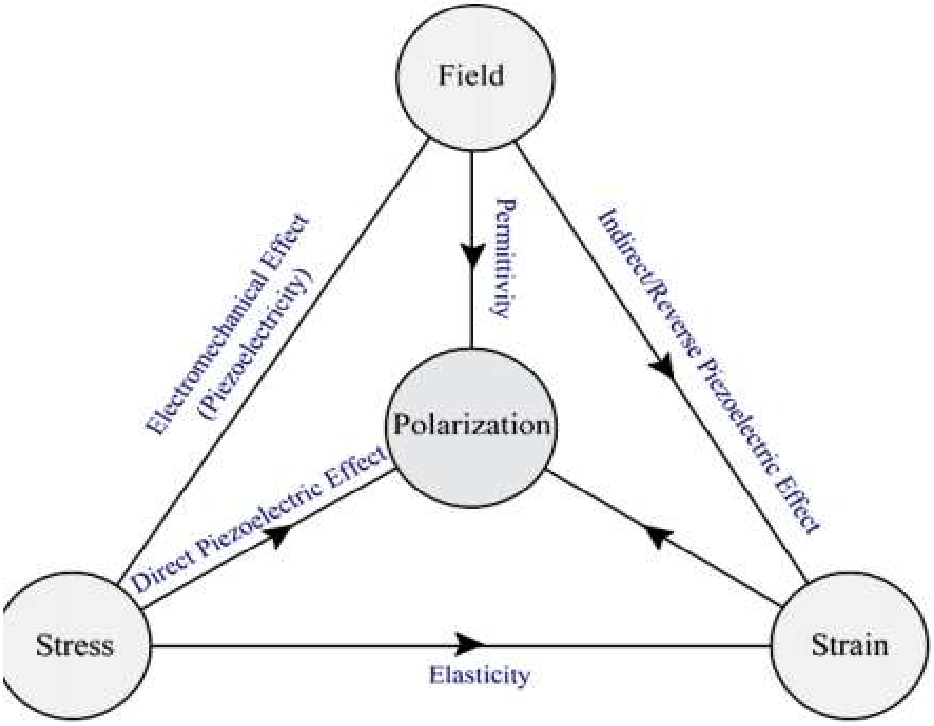

Figure 1.3 Piezoelectric Phenomena [32]

1.3 (a) Direct Piezoelectric Effect

This piezoelectric effect occurs while a piezoelectric material is under compression**.** In doing so, a piezoelectric material is between two metal plates. However, generating this piezoelectric material needs to be compressed, or its need to apply strain in the material. Hence, external mechanical stress is applied to this piezoelectric material to generate electricity. From Fig 2., we can see the two metal plates are on the top and bottom of the piezoelectric material like a sandwich and a voltage potential is created across the material. When the external load is applied and creates strain, both metal plates collect the charges, creating voltage that b is called piezoelectricity. This type of effect is called the direct piezoelectric effect. Many electronics devices use a direct piezoelectric effect, including microphones, pressure sensors, hydrophones.

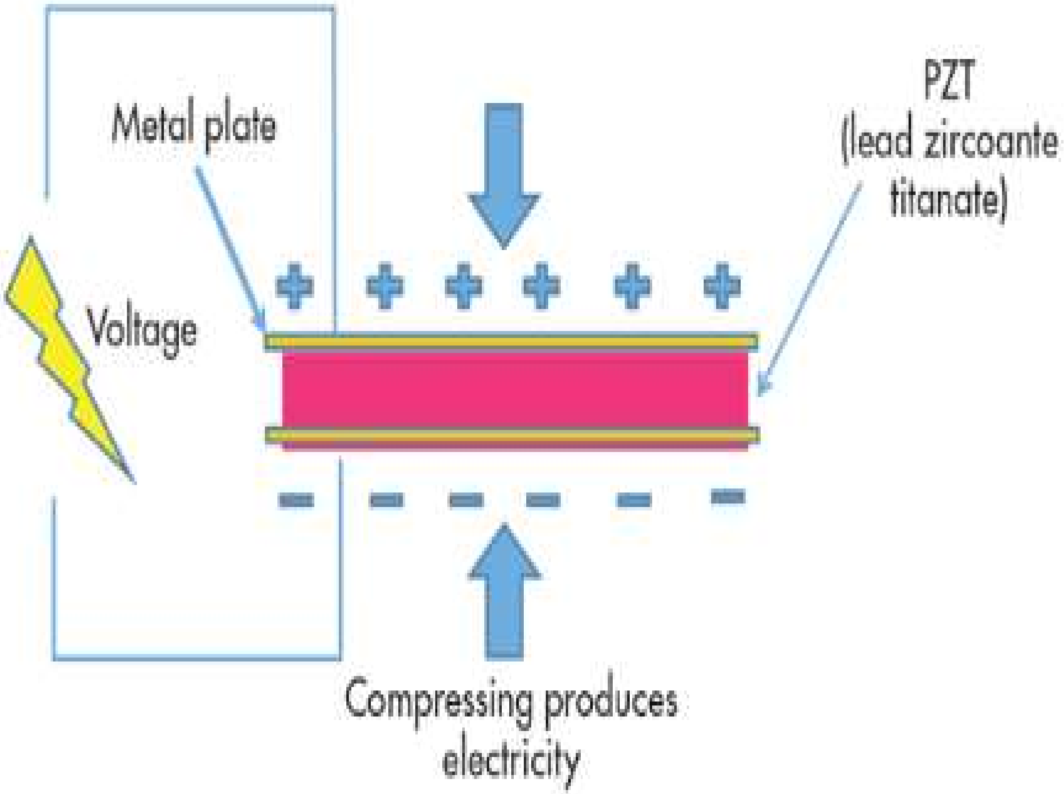

Figure 1.3 (a) Direct Piezoelectric Effect [32]

1.3 (b) Inverse Piezoelectric Effect:

The second type of piezoelectric effect is the Inverse Piezoelectric effect Fig.3. This effect works because when an electric voltage is applied as the piezoelectric material shrinks or expands, it tends to change its shape. The different devices, when manufactured, can produce acoustics sound waves. The inverse piezoelectric effect also has a good usage in aerospace research. Wing morphing design using the inverse effect of piezoelectric material has become very popular, which helped the aircraft wing change its shape in flight tan to fulfil the advanced aerodynamics performance requirement.

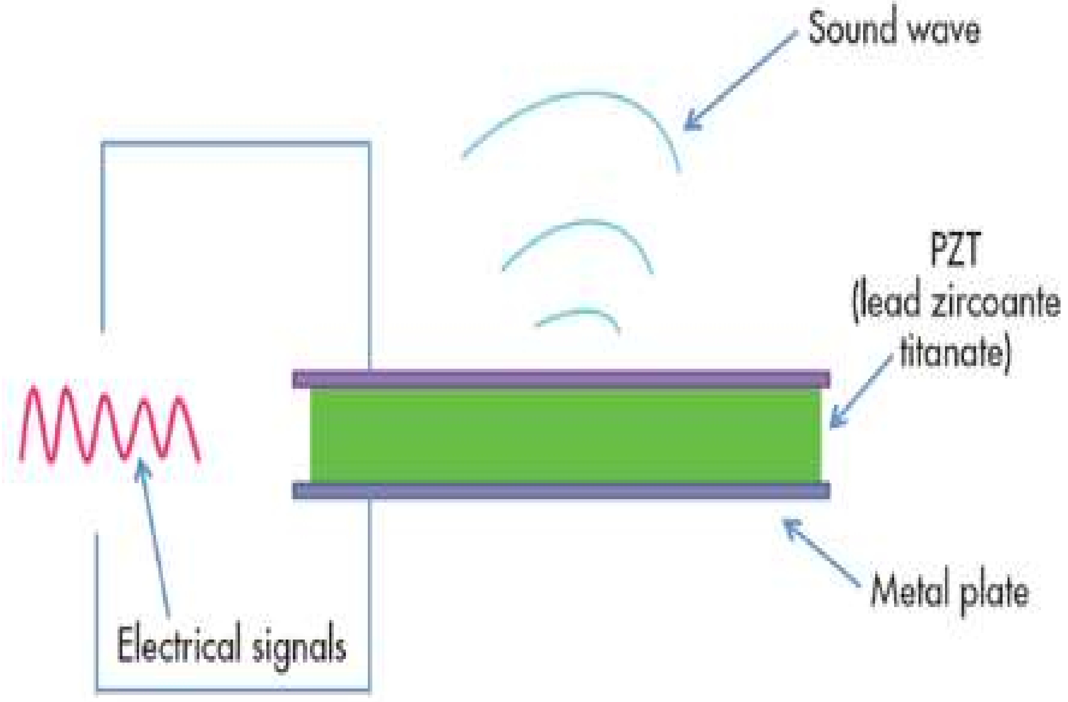

Figure 1.3 (b) Inverse Piezoelectric Effect [32]

1.4 Macro Fiber Composites (MFC)

Macro Fiber Composite is one type of piezoelectric material which NASA invented in 1999. This MFC can—though used for both low profile actuator and sensor—can provide very high flexibility, reliability, and efficiency compared to its price. This Macro Fiber composite comes from covering the rectangular piezo ceramic rods with layers of adhesive, electrode, and polyimide film like a sandwich. The electrodes attached to the film transfer the applied voltage to or from the piezo-ceramics rods.

When external electrical voltage is applied, it will bend or distorts materials to change their shape, whereas if it faces vibration or strain, it can produce electric voltage. Hence, it is considered an excellent energy harvester that can produce energy using mechanical vibration from the attached structure. This MFC is available from the SMART MATERIAL CORP. in d33 and d31 operational mode.

Figure 1.4 (a) MFC Energy Harvester (Courtesy: Smart Material)

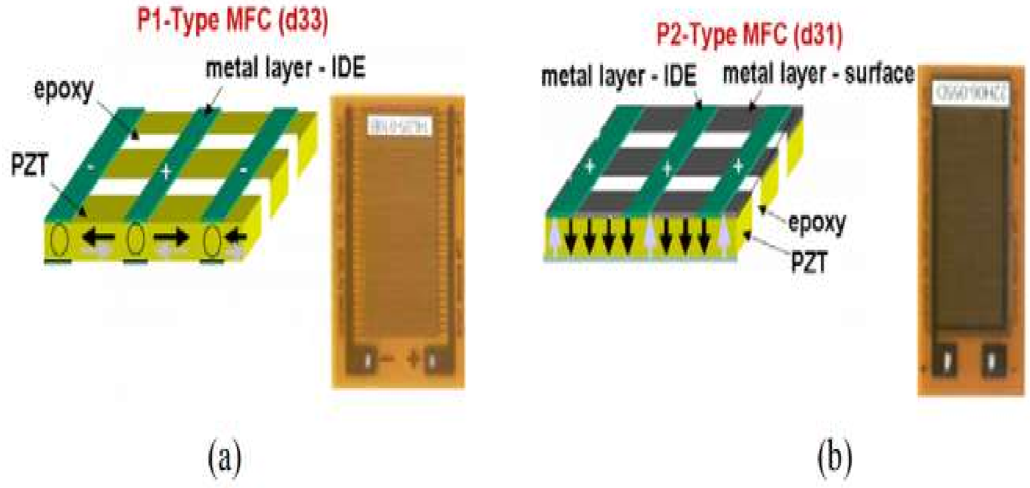

Figure 1.4 (b) P1 (a) And P2-Type (b) MFCs (Courtesy: Smart Material)

1.5 Research Objectives

Several studies investigate the vibration energy harvesting from piezoelectric macro fiber composites and wing morphing design to enhance model wing or UAV aerodynamics by using these MFC as actuators. However, this research limits its coverage to substrates or aerofoil configurations. However, to find out the best suitable configurations and dig further in this area, more details or a wide range of metal substrates and aerofoil configurations shall be investigated and tested.

This study proposed widening the investigation area, including three more substrates—copper, zinc alloy and galvanized steel**.** This study also compares the results with the earlier state of the art where brass, aluminum, and stainless steel were used as MFC substrates to find the maximum pick power. Similarly, for designing the wing morphing and active flow control of a thin aerofoil, the experimental and numerical results focused on the NACA 0014 aerofoil. However, in this study, the researchers want to validate the NACA 0012 aerofoil, and existing NACA 0014 aerofoil data obtained from computational and wind tunnel experimental data in terms of designing wing morphing and active flow control—with both computational and wind tunnel experimental data a view to designing an aileron free flying wing aircraft.

1.6 Overview of Study Content

The overview of this research project in figure 1.3 shows that the current research work will contain six chapters. The current or the ongoing chapter gives us a general introduction to the working principle of piezoelectric energy harvesting from residual/unused vibration and the method of harvesting this energy. The most crucial point to be noted is the application of a vibration/structural deformation to the piezoelectric material or macro fiber composites (MFC). It produces the electricity—and oppositely while applying an external voltage to the MFC—applied electric voltage deformation or shape change occurs to this MFC material. This process is a fundamental motivating concept to utilize this property to build or design wing morphing design to take advantage of inflight shape change of the wing to achieve enhanced aerodynamics efficiency.

Chapter 2 discusses the recent works performed in piezoelectric energy harvesting from vibration source or utilizing any other source of micro deformation along with the utilization of morphing wing concept utilizing these fantastic properties of shape-changing due to externally applied voltage. This chapter is all about a brief literature review. Chapter 3 details methodology, modelling, and experimental setup for this research and investigation. This project's computational and numerical simulation was described carefully and precisely, along with the significant challenges and findings in chapter 4. Chapter 5 discusses the results obtained from the numerical/computational simulations and their conformity with experimental results from the state of art. The researchers conclude and expect some future works in this area in the last part, which is chapter 06.

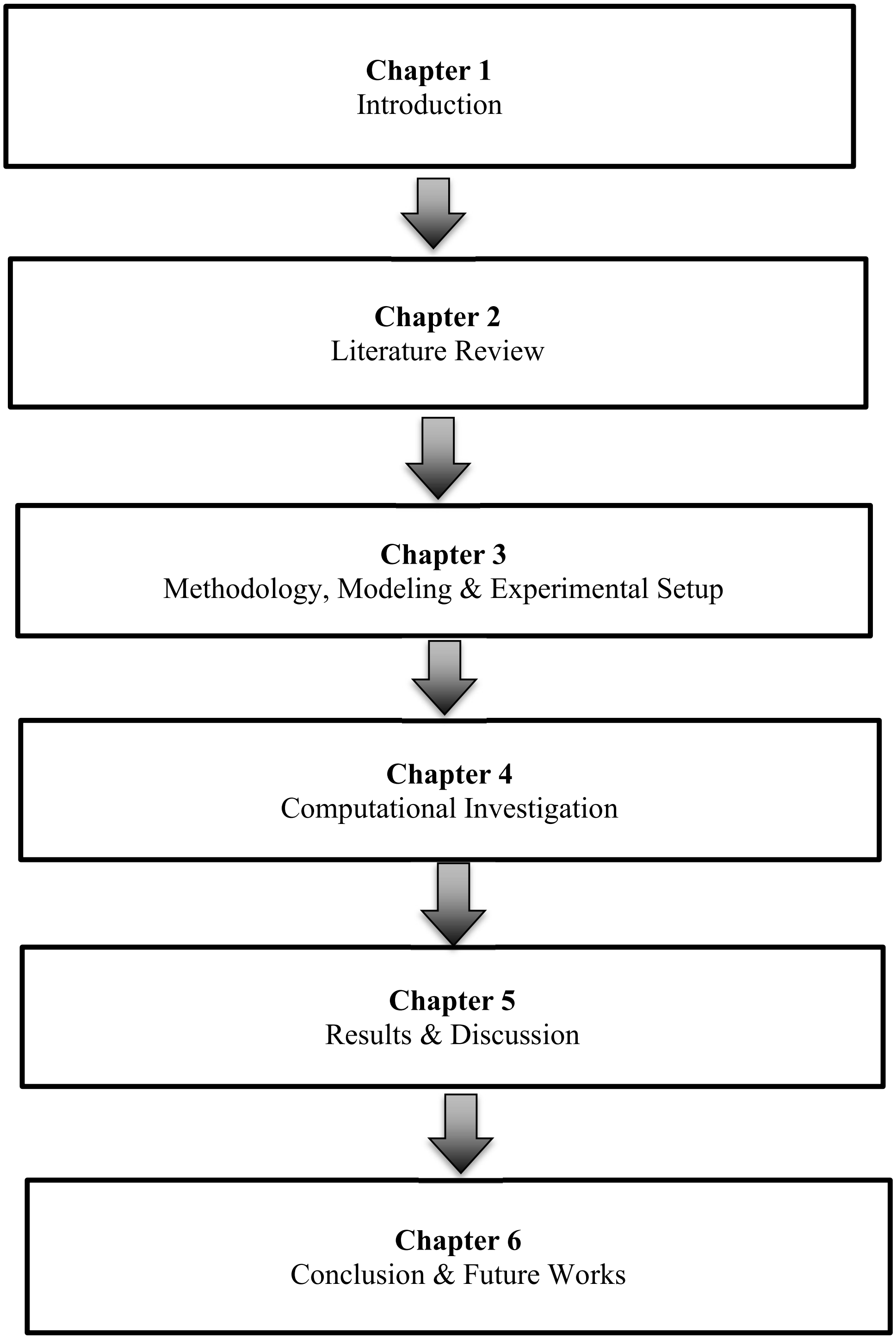

Fig.1.6 (a) Organization of the Chapters.

CHAPTER 2

LITERATURE REVIEWS

2.1 Piezoelectric Energy Harvesting and Wing Morphing Design

Sodano et al. (2004) published a review paper describing the development that took place throughout time in power harvesting using piezoelectric material and its future goal [1]. Schultz and Hyer (2004) did use the Macro Fiber Composites (MFC) to prepare possible morphing structures by controlling Bi-stable unsymmetrical composite laminates. [2] Discalea et al. (2007) proposed a method using ultrasonic guided waves that could monitor the health condition of the composite wing skin-to-spar joint in Unmanned Aerial Vehicles. The ultrasonic transmission strength via the joints was measured using computational and experimental measurements. The dispersive wave propagation issue was studied numerically using the semi-analytical finite element approach. Flexible Macro Fiber Composite (MFC) transducers aided in the experimental investigation. Ultrasonic measurements were de-noised and compressed using Discrete Wavelet Transform (DWT). The numerical and experimental test confirmed that across the defected bond, the ultrasonic strength of the transmission increased [3].

Park et al. (2005) detected subsurface delamination in a composite plate using piezoelectric Macro- Fiber Composites) to measure the frequency response function (FRF). A small projectile led to the creation of damage and delamination. The frequency response calculation assessed machines' conditions at a high-frequency range of 5-20 kHz. MFCs, as they sustained all impacts, is considerably more rugged than PZT. Identification of all damage states was possible with the damage feature [4]. Chiamori et al. (2008) proposed an integrated approach for identifying the structural damage of the pipeline. Using the Impedance and Lamb wave Propagation method, the connection damage in the flange joint and the location of surface damage in the main body of the pipeline were identified, respectively [5].

Sodano et al. (2005) used the idea of using rechargeable batteries with piezoelectric materials instead of capacitors. The energy of three different piezoelectric devices, the MFC, lead–zirconate–titanate (PZT), the Quick Pack (QP), recharged the nickel-metal hydride batteries. They discovered that PZT and QP could recharge the battery, while MFC was not well suited for power harvesting [6]. Similarly, Arms et al. (2007) discovered that when the usage level was too low, the energy used for consumption was less than the energy harvested. Piezoelectric materials generated power for microelectronics by converting the cyclic strain of pitch link operation [7].

Bilgen et al. (2007a) conducted an experimental, theoretical and computational analysis of remote-controlled aircraft for which morphing wing came from Macro Fiber Composites (MFC) [8]. Bilgen et al. (2007b) built an uncrewed aircraft using smart material. Likewise, their earlier work Macro Fiber Composites (MFC) was used to design the morphing wing [9]. Nuffer et al. (2007) investigated the reliability of MFC actuators. The experiment studied electromechanical cycling. They discovered that the possibility of failure due to degradation for the degradation mechanism up to 108 was unlikely. When used within specification, the result showed that the MFC showed high reliability [10].

Song et al. (2007) studied the energy harvesting device using macro-fiber composite material. They used a cantilever beam as a harvesting device made up of MFC material. The modelling, design, theoretical and experimental characteristics of a cantilever beam acting as an energy harvesting device was studied. With the governing equations of motion energy harvesting devices, they theoretically gained two MFC patches. Moreover, their study showed that it is possible to obtain the maximum power using a theoretical model. The theoretical study showed that the maximum power of energy harvesting devices increased when the beam's thickness, width, and density also increased. The study also showed an indirect relationship between beam length and maximum power. The effect of a wire connection between two MCF patches underwent further investigation, and the researchers discovered that a series connection was better for producing maximum power while generating maximum current parallel connection. Furthermore, it discovered that d31 could be better for charging a battery than d33 [11].

Daue and Kunzmann (2008) discovered that MFCs are well suited for directly utilizing vibrational waste present in the environment and harvesting the energy. Low overall cost makes PZT competitive with batteries when used with lower power applications [12]. In Erturk et al. (2008) study, an electromechanical model with distributed parameters can predict the electrical and mechanical response of MFC unimorph. The model based on a closed-form solution for monothilic uniform showed the capability to predict the coupled dynamics over a varying range of load resistance. Similarly, it showed that MFC with aluminum substrate generated the maximum peak power at resonance than those with brass and stainless steel. A couple of analytical models aided the successful prediction of experimental results. The preliminary result of the wind tunnel experiment came from flow morphing air coil to piezoelectric energy harvesting [13].

Anton and Inmam (2008) examined vibration and solar energy harvesting capability in a mini UAV. They discovered that both vibration and solar energy harvesting devices showed the capability to charge energy storage devices [14]. Yang et al. (2009) used a cantilever beam with MFC patches and calculated its capabilities in energy harvesting. The Finite Element Model (FEM) development came from comparing experimental results. Combined simulation tools, electronic design automation (EDA), and FEM were found to be efficient for optimizing and evaluating MFC-based energy harvesting systems [15].

Song et al. (2010) studied the modelling, design, theoretical and experimental characteristics of a cantilever beam acting as an energy harvesting device. The theoretical model-based study showed an increase in maximum power with increased beam thickness, width and density. Similarly, the maximum power decreased when the length of the beam increased. When the two patches of MFC are in a series, it showed better results in producing maximum power than when connected in parallel. When connected parallelly, it generated maximum current [16].

Debiasi et al. (2013) conducted a follow-on study using Macro Fiber Composite actuator to change the airfoil model's upper and lower surface shape with closely similar geometry of a NACA 0014 [17]. Their other paper investigated the Deformation of the Upper Surface of an Airfoil by Macro Fiber Composite Actuators [18]. Thornburhg et al. (2014) studied the usage of continuous trailing edge flaps (CTEFs) as the primary flight control of a helicopter [20]. Ofori-Atta (2014) experimented with Morphing Wing Aircraft with the wing designed using Macro Fiber Composites [21]. Rosario et al. (2016) performed the numerical and experimental validation of the mechanical behavior of hybrid specimens made up of thin carbon and glass substrate in which Macro Fiber Composites (MFC) patches are glued [22].

Thornburgh et al. (2016) performed both the bench test and wind tunnel test of a prototype rotor-blade section with an integrated Continuous Trailing-Edge Flap (CTEF) [23]. Grzybek and Micek performed the experimental investigation on energy harvesting from vibration energy of buildings using MFC. The investigation concluded that establishing the resonant frequency of the piezoelectric beam generator is essential for the vibration frequency and vibration amplitude of mechanical structures [24]**.** Shi et al. (2017) proposed a fabrication method and process to integrate piezoelectric electric harvesting (EH) elements and carbon-fibre composite structure. The energy harvested by different integration methods was characterized by performing dynamic vibration tests under varying vibration frequency and applied mechanical loading. Similarly, the energy harvested by mechanical vibrations came from an analytical model. They found that the co-curing method showed better performance than the mechanical bonding approach at a frequency of 10 Hz, showing an improvement of 14.3%. The co-curing through sweep test also showed its potential at higher frequencies [25]**.**

Sun et al. (2018) demonstrated the potential of energy harvesting from water flow in an open channel with MFC. Hamadan et al. (2018) investigated the MFC bonded factor for understanding the behavior that could influence the micro-energy harvester's performance. The study found that bonded technique was the most influencing factor over the vibration range of 10-90 Hz, suggesting bonded to structure as a better technique to maximize micro-energy harvesting. They discovered that Structural Health Monitoring could also be applied simultaneously with a micro-energy harvesting system [27]. Gao et al. (2019) proposed a device that converted the rotary motion of the knee joint to linear motion and again to bending motion using a bending beam. The experimental result found that a lightweight harvester could generate 1.60 mW power without walking [28]. Cadogan et al. (2004) developed Morphing Inflatable Wing for Compact Package Unmanned Aerial Vehicles using Macro Fiber Composites [29]. In their second paper, Debiasi et al. (2012) investigated the Deformation of the Upper Surface of an Airfoil by Macro Fiber Composite Actuators [30]. A simple cantilever energy harvester can produce significant energy with deformation or vibration. In 2002, Flynn and Sander had imposed the mechanical stress limit of this type of energy harvester. Their analysis with the piezoelectric material found that a mechanical stress-limited work cycle was 330W/cm3 at 100 kHz for PZT-5H [33]. Similarly, Elvin et al. (2001) conducted an experimental investigation of a PZT model with theoretical modelling of a beam element. [34]. Roundy et al. (2004) conducted a series of experiments with a different vibration energy harvester for low-level vibration generated from the household and the office environment. For a given vibration level or mechanical vibration being applied piezoelectric energy conversion is significantly higher than the MEMS [35-38] depicts in figure 4.

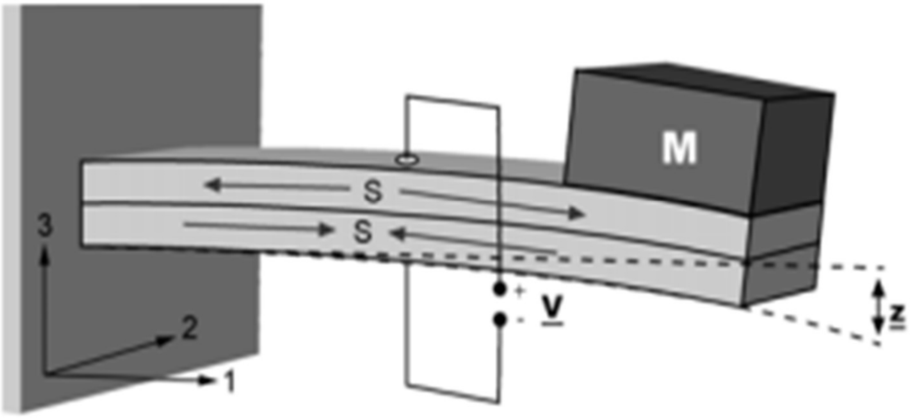

Figure 2.1 (a) P1 (a) A cantilever with two layers bender [35]

The research group of Inman's had published about ten papers based on vibration energy harvesting using PZT and MFC. Sodano et al. (2003, 2004) investigated three types of piezoelectric devices as a part of their experiment to see which one is better for recharging a discharged battery[39-40]. Shen et al. (2009) arrived with a PZT piezoelectric cantilever, a micromachined Si proof mass for a low-frequency vibration energy harvesting application [41]**.** Lieu et al. (2008) **d**eveloped a thick film array of power generator piezoelectric cantilevers to improve frequency flexibility and power output [42]**.** Similarly, Choi et al. (2006) revealed the improved performance concerning electrical power and output voltage to resistance load [43].

Kim et al. (2005) constructed a cymbal structure for micro energy harvesting that could produce a sizeable in-plane strain under the external force applied in a transverse direction [44]**.** Li et al. (2011) proposed two ring-type piezoelectric stacks, where its construction came from one pair of the bow-shaped elastic plate and one shaft that was pre-compressed [45] in figure 5.

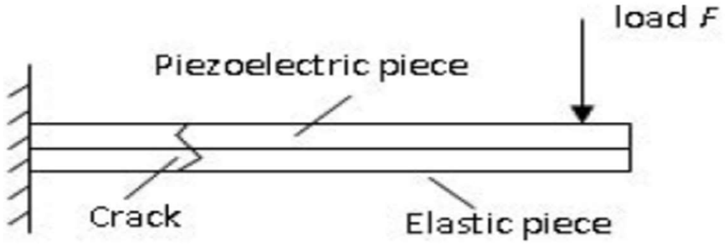

(a) Cantilever type

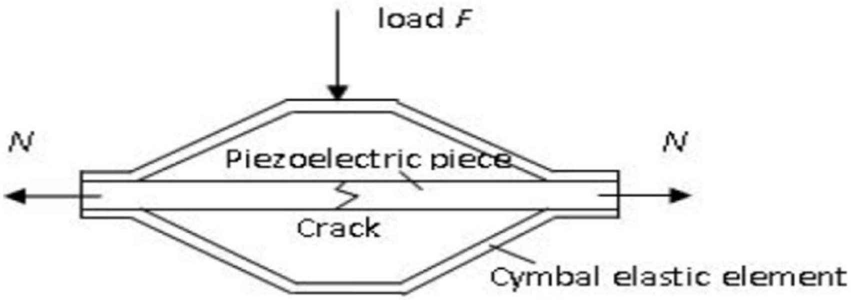

(b) Cymbal type^{24}

Figure 2.1 (b) Conventional piezoelectric energy harvester [46]

Another research conducted by Adhikari et al. (2009) published that a stack type piezoelectric transducer can produce a large amount of electrical energy because of its d33 mode and having multi-stacking of piezoelectric materials layer [46]. In 2006, Lefeuvre and other researchers proposed a synchronized switch damping (SSD) in vibrational piezoelectric energy harvesting, as shown in figure 6 [47].

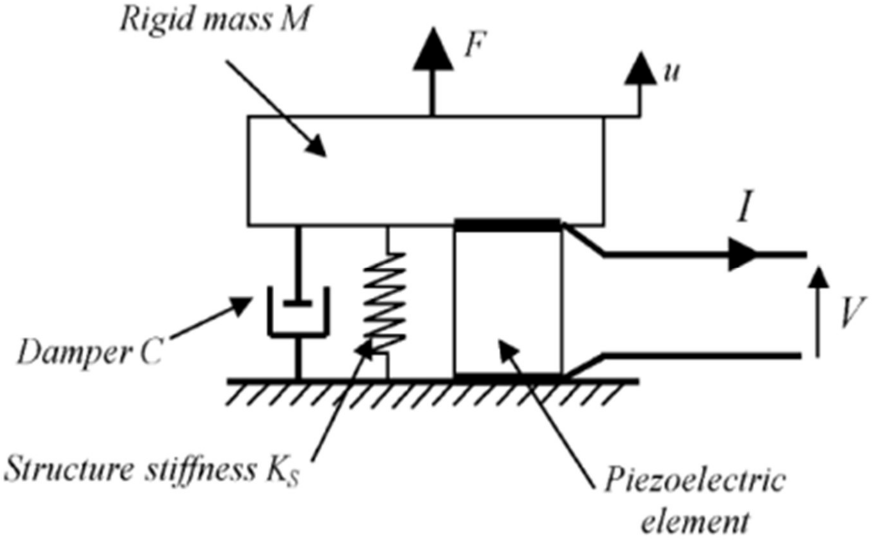

Figure 2.1 (c) Model of vibrating structure with a piezoelectric element [47]

Yoon et al. (2005) developed a curved piezoceramic structure to improve efficiency, keeping in mind that shell structure can generate a tremendous amount of strain than a flat plate, shown in figure 7 [48]. In a different study, Yoon et al. (2008) utilized a pneumatic shock machine to experiment on ring-shaped PZT-5A elements. They found the relationship between the energy transfer efficiency and the normalized impulse [49]. In 2007, Chen and his co-researchers investigated the piezoelectric shell of polarized ceramics under torsional vibration [50]. Erturk and

Inman (2008) proposed an improved mathematical model to correct the oversimplified issues related to a mathematical formulation like piezoelectric coupling, physical, low fidelity, and base motion modelling [51].

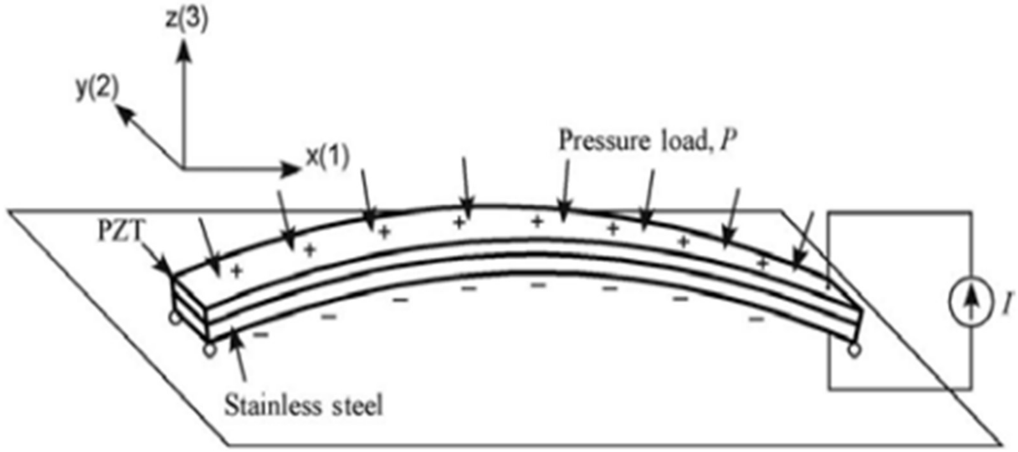

Figure 2.1 (d) Curved PZT unimorph excited in d31-mode by a normal distributed force [48]

The same research team proposed a correction factor for a single degree of freedom base excitation model [52]. Their research also proposed a close form analytical solution for biomorph cantilever configuration where piezoceramic layers are in series and parallel connections [53].

Marqui et al. (2009) proposed an electromechanically coupled finite element (FE) plate model based on Kirchhoff plate assumptions that also account for the effect of conductive electrodes to predict the electrical power output of piezoelectric energy harvester plates [54]. Renno et al. (2009) used an inductor and resistive load to optimize the piezoelectric vibration [55].

Pouline et al. (2004) compared an electromagnetic system made of a magnet in translation with a coil and piezoelectric system and predicted a substantial similarity and duality in signal level [56]. In 2007, Ajitsaria and other researchers discovered that the comparison between the experimental results and simulation is satisfactory based on the Euler–Bernoulli beam theory and Timoshenko beam equations for voltage and power generation [57].

Hu et al. (2007) proposed modelling a piezoelectric energy harvester/energy harvesting method as an integrated electromechanical system by characterizing the interaction between the harvesting structure and the storage circuit with a nonlinear rectifier [58]. In 2006, Shu and Lein optimized energy conversion efficiency under steady-state conditions for a rectified piezoelectric power harvester and concluded that the optimization criteria depend upon the relative strength of the electromechanical coupling [59].

In 2009, Marzencki and other researchers developed a wideband adaptive system by applying mechanical nonlinear strain stiffening. Their experiment claimed that their proposed solution was almost accurate for heavy pieces of industrial machinery surveillance where vibration with high amplitude is usually available [60].

CHAPTER 3

METHODOLOGY, MODELING AND EXPERIMENTAL SETUP

3.1 Mathematical Modeling

Erturk and Inman (2008, 2009) represented the primary mathematical modelling for the unimorph cantilever with a monolithic piezoceramic layer excited because of the vibration or motion of the base [61,62]. However, later this mathematical modelling was extended and made robust for the biomorph configuration after being tested. Mathematical modelling assumptions were made based on the Euler-Bernoulli beam theory assumptions). Shear deformations and rotating inertia effects, according to theory, are insignificant. The mechanical behaviors of both the substrate and the piezoelectric layer are linearly elastic, and the base vibration was regarded minimal. Hence for the metal substrate, epoxy and the Kapton layer, Hooke's law was modified:

$$T_s = Y_s S_s, T_e = Y_e S_e, T_k = Y_k S_k \tag{1}$$

Here, T is the bending stress component, S is the bending stress component, and Y is the young's modulus of the isotropic layer of the substrate, epoxy and Kapton**,** respectively**.** The piezoceramic material used follow the following linear relation obtained from state of the art [63].

$$\begin{pmatrix} T_3 \\ D_3 \end{pmatrix} = \begin{bmatrix} \bar{c}^E{}_{33} & -\bar{e}_{33} \\ \bar{e}_{33} & \bar{\varepsilon}^S{}_{33} \end{bmatrix} \begin{pmatrix} S_3 \\ E_3 \end{pmatrix} \tag{2}$$

Where T3 is the stress component, D3 is the electric displacement component, S3 is the strain, and E3 is the electric field component. Here, the bar is in the plane-stress conditions, and it does not denote the elasticity component. From figure 3.1, we can define that; the direction of the mechanical strain and the electric field is the same, and it is directed to the beam's longitudinal (x) direction [13].

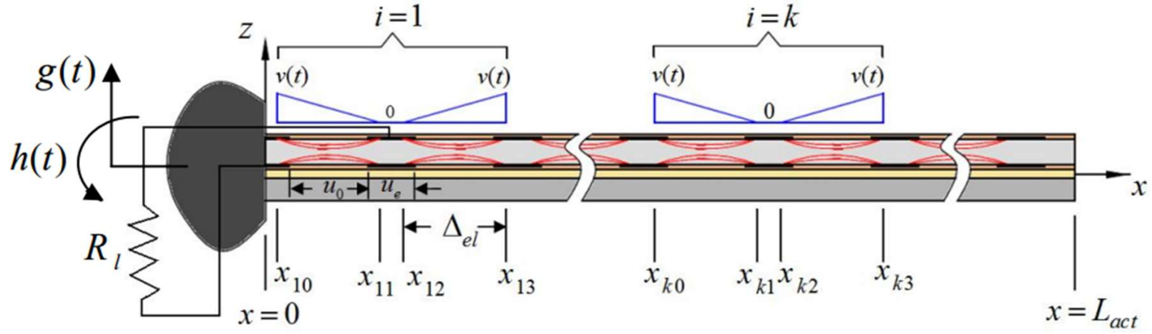

Fig 3.1 Base excitation applied to the unimorph MFC Cantilever [13]

Here, an approximation is applied such that MFC and the Epoxy layer are boned by the substrate material. This substrate layer will not produce any shear in between these two layers.

3.2 Mechanical Equations for Coupled Biomorph:

The MFC with the cantilever beam configuration shown in figure 3.1 is governed by the partial differential equations described below [13]:

$$\frac{\partial^2 M(x,t)}{\partial x^2} + c_s I \frac{\partial^5 w(x,t)}{\partial x^4 \partial t} + c_a \frac{\partial w(x,t)}{\partial t} + m \frac{\partial^2 w(x,t)}{\partial t^2} = 0 \qquad \textbf{(3)}$$

Here M(x,t) defines the bending moment acting internally due to strain rate damping. W(x,t) is the deflection acting in the transverse direction, C_sI defines the strain rate. Viscous damping coefficient is defined by C_a. The excitation applied to the basement of the experiment setup, or the beam can be denoted as

$$W_b(x,t) = g(t) + xh(t) \tag{4}$$

On the above equation, g(t) is the translation motion of the base in the transverse direction, superimposed small rotation of the base is denoted by h(t). Transverse displacement of the experimental beam with respect to the frame is defined by the following equation:

$$w(x,t) = w_b(x,t) + w_{rel}(x,t) \tag{5}$$

Here in equation (5), W_{rel} (x,t) defines the displacement occurs in the transverse direction with compare to the base which is moving. We can obtain the Wb (x,t) from the equation (4) discussed above. We will put the equation (5) to the equation (3). By doing so we can obtain a partial differential equation below which will represented in terms of W_{rel}(x,t).

$$\frac{\partial^2 M(x,t)}{\partial x^2} + c_s I \frac{\partial^5 w_{rel}(x,t)}{\partial x^4 \partial t} + c_a \frac{\partial w_{rel}(x,t)}{\partial t} + m \frac{\partial^2 w_{rel}(x,t)}{\partial t^2} = -\frac{\partial^2 w_b(x,t)}{\partial t^2} - C_a \frac{\partial w_b(x,t)}{\partial t} \tag{6}$$

As per the above equation, if we express the strain component in terms of curvature and the electric field in terms of voltage, we can perform the integration of the moment of axial stress over the whole cross section of the beam.

$$\mathrm{YI}\,\frac{\partial^4 w(x,t)}{\partial x^4}+c_s I\,\frac{\partial^5 w(x,t)}{\partial x^4 \partial t}+c_a\,\frac{\partial w(x,t)}{\partial t}+m\,\frac{\partial^2 w(x,t)}{\partial t^2}+v(t)\,\frac{d^2\Gamma(x)}{\partial x^2}=-m\,\frac{\partial^2 w_b(x,t)}{\partial t^2}-C_a\,\frac{\partial w_b(x,t)}{\partial t} \quad \mathbf{(7)}$$

Here the bending stiffness (YI) can be obtained from the transformation of the cross section. Γ(x) is the electric potential, and they are spatially distributed. Here in the equation (8), ϑ is defined as the coupling constant. Coupling constant (ϑ)can be expressed by:

$$\Gamma(x)=\vartheta\sum_{i=1}^{N_e}\left\{\left(1+\frac{x-x_{i0}}{x_{i0}-x_{i1}}\right)\left[H(x-x_{i0})-H(x-x_{i1})\right]+\left(\frac{x-x_{i2}}{x_{i3}-x_{i2}}\right)\left[H(x-x_{i2})-H(x-x_{i3})\right]\right\} \quad \mathbf{(8)}$$

The coupling constant (ϑ) is being given by:

$$\vartheta=-\frac{\bar{e}_{33}b_{pt}[\left(h_d-\alpha h_p\right)^2-\left(h_c+\alpha h_p\right)^2}{2\Delta_{el}} \quad \mathbf{(9)}$$

Here, in equation number (9) α is an empirical correction factors which is responsible for reducing the thickness of piezoceramics which is mainly responsible for the piezoelectrically induced bending moment with non-uniform electric field [13].

3.3 Electrical Equations for Coupled Biomorph

From the above figure 3.1, we can notice that an electric load (R_l) is connected in the electrical circuit [13]. For this circuit where the piezoceramic operates, it will have an admittance ($1/R_l$) [13]. Hence, a per following the IEEE standard for piezoelectricity, we can write the following equation [63].

$$\frac{d}{dt}\left(\int_{\boldsymbol{A}} \boldsymbol{D}.\boldsymbol{n} da\right) = \frac{v(t)}{R_l} \tag{10}$$

Here v (t) is the amount of voltage available through the resistive load, D is the electric displacement vector, n is the unit outward normal on the electrode surface and the integration is performed over the electrode area (Figure 3.2) [13].

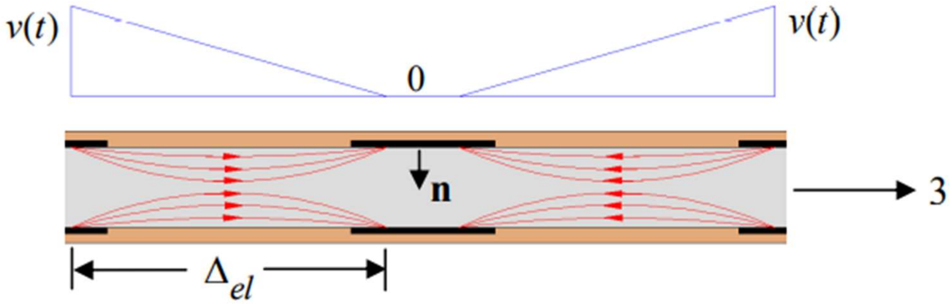

Fig. 3.2 Non-uniform electric field lines and the electric potential distribution [13]

From figure 3.2 it can be noted that, electric field lines are in the x direction. However, with the electrode surface, they usually make an angle in the electrodes vicinity. As a result, a correction factor (*β*) is taken into consideration to deal with this angle generation between the electric displacement component and the surface normal on the electrode surface [13]. Once we submit the equations obtained in equation (2) to the equation (10), the following equations can be built up.

$$C_p \frac{dv(t)}{dt} + \frac{v(t)}{R_l} = -(h_{pc} + \frac{h_p}{4} \int_{\boldsymbol{A}} \bar{e}_{33} \frac{\partial^3 w_{rel}(x,t)}{\partial x^2 \partial t} \beta dA - (h_{pc} - \frac{h_p}{4}) \int_{\boldsymbol{A}} \bar{e}_{33} \frac{\partial^3 w_{rel}(x,t)}{\partial x^2 \partial t} \beta dA \tag{11}$$

Here, capacitance of the MFC is Cp, h_{pc} is defined as the center of the piezo ceramics from the neutral axis and *β* is the correction factor. The value of β is near about 0.5 for M 8507 P1 configuration of Macro Fiber Composites (MFC). The previously discussed equation 11 can be rewritten as equation 12 below [13].

$$C_p \frac{dv(t)}{dt} + \frac{v(t)}{R_l} = -2\beta \bar{e}_{33} h_{pc} \int_{\boldsymbol{A}} \frac{\partial^3 w_{rel}(x,t)}{\partial x^2 \partial t} \beta dA \tag{12}$$

Based on the region covered by the MFC, the equation (12) obtained earlier can be extended in the following equation (13) as per the figure descript (fig. 3.1).

$$C_p \frac{dv(t)}{dt} + \frac{v(t)}{R_l} = -2\beta \bar{e}_{33} h_{pc} b_{pt} (\int_{x_{i0}-\frac{u_e}{4}}^{x_{i0}+\frac{u_e}{4}} \frac{\partial^3 w_{rel}(x,t)}{\partial x^2 \partial t} dx + \int_{x_{i1}-\frac{u_e}{4}}^{x_{i2}+\frac{u_e}{4}4} \frac{\partial^3 w_{rel}(x,t)}{\partial x^2 \partial t} dx + \int_{x_{i3}-\frac{u_e}{4}}^{x_{i3}+\frac{u_e}{4}4} \frac{\partial^3 w_{rel}(x,t)}{\partial x^2 \partial t} dx \tag{13}$$

3.4 Modal Analysis of Bonded MFC:

Due to applied vibration, the MFC response compared to its base can be depicted as an uniformly convergent eigenfunction as in equation 14 [13].

$$w_{rel}(x,t) = \sum_{r=1}^{\infty} \eta_r(t)\, \phi_r(x) \tag{14}$$

Mass normalized eigenfunctions here are $\phi_r(x)$ and $\eta_r(t)$. Taking into consideration proportional damping assumption, eigenfunctions of the proportionally damped system become the eigenfunctions of the respective undamped system [13].

$$\phi_r(x) = \sqrt{(\frac{1}{mL}\left[\frac{cosh\lambda_r}{L}x - \frac{cos\lambda_r}{L}x - \sigma_r\left(\frac{sinh\lambda_r}{L}x - \frac{sin\lambda_r}{L}x\right)\right]} \tag{15}$$

On the above equation, λ_r is a dimensionless frequency number, and we can obtain it from the following equation.

$$1 + \cos\lambda \cosh\lambda = 0 \qquad \textbf{(16)}$$

And the value of σ_r can be obtained from the equation (17).

$$\sigma_r = \frac{sinh\lambda_r - sin\lambda_r}{cosh\lambda_r + cos\lambda_r} \qquad \textbf{(17)}$$

Undamped natural frequency ω_r can for the *rth* mode can be written as

$$\omega_r = \lambda_r^2 \sqrt{\frac{YI}{mL^4}} \qquad \textbf{(18)}$$

For the light mechanical damping, it is assumed to be the resonance frequency of the unimorph. In this case, the following orthogonality conditions can be satisfied by the mass-normalized eigenfunctions.

$$\int_{x=0}^{L} m\phi_s(x)\phi_r(x)dx = \delta_{rs} \qquad \textbf{(19)}$$

$$\int_{x=0}^{L} YI\phi_s(x)\frac{d^4\phi_r(x)}{dx^4}dx = \omega_r^2\delta_{rs} \qquad \textbf{(20)}$$

3.5 Modal Coordinates and Governing Equations

Electromechanically coupled equations for the unimorph cantilever beam under base excitation are shown in equation (6) and equation (13). Now, if we substitute equation (14) to the equation (6), and if we apply the orthogonality conditions of the eigenfunctions described earlier, the following equation can be derived.

$$\frac{d^2\eta_r(t)}{dt^2} + 2\zeta_r\omega_r\frac{d\eta_r(t)}{dt} + \omega_r^2\eta_r(t) + \varkappa_r v(t) = N_r(t) \quad \textbf{(21)}$$

Here, $\varkappa_r$ is the modal coupling term and ζ_r is the mechanical damping ratio. The mechanical damping here is the combined effect of strain rate damping and viscous air damping together.

$$\varkappa_r = \int_0^L \phi_r(x)\frac{d^2\Gamma(x)}{dx^2}dx = \vartheta\sum_{i=1}^{N_e}\left(\frac{\phi_r(x_{i0})-\phi_r(x_{i1})}{x_{i0}-x_{i1}} + \frac{\phi_r(x_{i2})-\phi_r(x_{i3})}{x_{i3}-x_{i2}} + \frac{d\phi_r(x)}{dx}\right) \quad \textbf{(22)}$$

From the following equation (23), we can presume that strain rate damping is proportional bending stiffness of the beam and mass per unit length to be proportional to the air damping.

$$\zeta_r = \frac{c_s I\omega_r}{2Y} + \frac{c_a}{2m\omega_r} \quad \textbf{(23)}$$

Equation (24) defines the modal mechanical function discussed in equation (21).

$$N_r(t) = N_r^m(t) + N_r^c(t) \quad \textbf{(24)}$$

The component of mechanical base excitation is described by the following two equations (25) & (26)

$$N_r^m(t) = -m\left(\gamma_r^w \frac{d^2g(t)}{dt^2} + \gamma_r^\theta \frac{d^2h(t)}{dt^2}\right) \tag{25}$$

$$N_r^c(t) = -c_a(\gamma_r^w \frac{dg(t)}{dt} + \gamma_r^\theta \frac{dh(t)}{dt}) \tag{26}$$

Here,

$$\gamma_r^w = \int_{x=0}^{L} \phi_r(x)dx \tag{27}$$

$$\gamma_r^\theta = \int_{x=0}^{L} x\phi_r(x)dx \tag{28}$$

Usually in case of energy harvesting in the air medium, as the external damping exerted by air is very negligible hence $N_r^c(t) = 0$.

Now, if we substitute equation (14) to the equation (13) we get the following equation (29).

$$C_p \frac{dv(t)}{dt} + \frac{v(t)}{R_l} = \sum_{r=1}^{\infty} \kappa_r \frac{d\eta_r(t)}{dt} \tag{29}$$

Here equation (29) and (21) are couple equations for piezoelectrically unimorph modal.

3.6 Electromechanical Response for Harmonic Excitation:

Base motion is $g(t) = Y_0 e^{j\omega t}$ and $h(t) = \theta_0 e^{j\omega t}$ as a result it can be written $w_b = (Y_0 + x\theta_0)e^{j\omega t}$ at that situation mechanical response of the system/modal and the voltage response can be written as:

$$\eta_r(t) = H_r e^{j\omega t} \tag{30}$$

$$v(t) = V_0 e^{j\omega t} \tag{31}$$

Here, Y_0 & θ_0 are the rotation and translation of the base respectively while ω is the driving frequency and j is the imaginary number [13]. Here in the equation number (30) & (31), H_r is the complex mechanical modal and V_0 is the amplitude of complex voltage response.

$$(\omega_r^2 - \omega^2 + 2\zeta_r\omega_r)H_r + \varkappa_r V_0 = F_r \tag{32}$$

By using equation (30) & (31) and following their relation, equation (21) produces the equation (32) where in the equation (32)

$$F_r = m\omega^2\left(\gamma_r^{w} Y_0 + \gamma_r^{\theta}\theta_0\right) - jc_a\omega(\gamma_r^{w} Y_0 + \gamma_r^{\theta}\theta_0) \tag{33}$$

Following the same way from equation (29), we get the equation (34)

$$\left(\frac{1}{R_l} + j\omega C_p\right)V_0 = j\omega\sum_{r=1}^{\infty}\kappa_r H_r \tag{34}$$

To find out the complex voltage amplitude (V_0) yielding, we can find out the H_r value from the equation (32) and by putting this value again in equation (34).

$$v(t) = \frac{\sum_{r=1}^{\infty}\frac{j\omega\kappa_r F_r}{\omega_r^2-\omega^2+j^2\zeta_r\omega_r\omega}}{\frac{1}{R_l}+j\omega C_p+\sum_{r=1}^{\infty}\frac{j\omega\quad_r x_r}{\omega_r^2-\omega^2+j^2\zeta_r\omega_r\omega}}\, e^{j\omega t} \tag{35}$$

After doing so, the way we discovered the value of H_r by putting V_0 into the equation (32), similarly the following equation (36) can be derived from the equation (14).

$$W_{rel}(x,t) = \sum_{r=1}^{\infty}[(F_r - x_r \frac{\sum_{r=1}^{\infty} \frac{j\omega\kappa_r F_r}{\omega_r^2 - \omega^2 + j^2\zeta_r\omega_r\omega}}{\frac{1}{R_l} + j\omega C_p + \sum_{r=1}^{\infty} \frac{j\omega\kappa_r x_r}{\omega_r^2 - \omega^2 + j^2\zeta_r\omega_r\omega}}) \frac{\phi_r(x)e^{j\omega t}}{\omega_r^2 - \omega^2 + j^2\zeta_r\omega_r\omega}] \quad \textbf{(36)}$$

3.7 Unimorph Model Verification

In simple terms, the component of base excitation because of external damping is negligible and the uniform substrate configuration does not rotate ($h(t) = \theta_0 e^{j\omega t} = 0$), then equation (33) can be written in a reduced format like equation (37) below.

$$F_r = \gamma_r^w m\omega^2 Y_0 \quad \textbf{(37)}$$

By using equation (35), voltage output to the base acceleration frequency response function (FRF) can be obtained inequation (38).

$$\mu(\omega) = \frac{v(t)}{-\omega^2 Y_0 e^{j\omega t}} = \frac{\sum_{r=1}^{\infty} \frac{-j\omega\kappa_r\gamma_r^W}{\omega_r^2 - \omega^2 + j2\zeta_r\omega_r\omega}}{\frac{1}{R_l} + j\omega C_p + \sum_{r=1}^{\infty} \frac{j\omega\kappa_r x_r}{\omega_r^2 - \omega^2 + j2\zeta_r\omega_r\omega}} \quad \textbf{(38)}$$

Following the similar way, relative displacement with respect to the base acceleration can be obtained from equation (36).

$$(\omega, x) = \frac{w_{rel}(x,t)}{-\omega^2 Y_0 e^{j\omega t}} = \sum_{r=1}^{\infty}[(\gamma_r^W - \varkappa_r \frac{\sum_{r=1}^{\infty} \frac{-j\omega\kappa_r\gamma_r^W}{\omega_r^2 - \omega^2 + j2\zeta_r\omega_r\omega}}{\frac{1}{R_l} + j\omega C_p + \sum_{r=1}^{\infty} \frac{j\omega\kappa_r x_r}{\omega_r^2 - \omega^2 + j2\zeta_r\omega_r\omega}}) \frac{-m\phi_r(x)}{\omega_r^2 - \omega^2 + j2\zeta_r\omega_r\omega}] \quad \textbf{(39)}$$

Here, the point to note is, absolute velocity of the beam at a very specific point of interest where $x = L_m$ is measured by the vibrometer. Hence, to modify the equation (39), it shall produce the absolute velocity response as in equation (40).

$$\psi_{modified}(\omega, L_m) = \frac{\frac{dw(L_m,t)}{dt}}{-\omega^2 Y_0 e^{j\omega t}} = \frac{\frac{d}{dt}[Y_0 e^{j\omega t} + w_{rel}(L_m,t)]}{-\omega^2 Y_0 e^{j\omega t}} = \frac{1}{j\omega} + j\omega\psi(\omega, L_m) \quad \textbf{(40)}$$

It is evaluated on the specific measurement point by the laser vibrometer [13].

3.8 Experimental Setup:

MFC unimorph is excited from its base through an LDS electromagnetic shaker. A low mass accelerometer measured the base harvester's acceleration (PCB U352C22). A laser vibrometer [13]The response of the velocity of the harvester at the free end. The experimental setup is shown in figure 3.8 (a).

Fig 3.8. Experimental setup to test MFC Unimorph [13]

For the experimental session, resistive loads' testing reached 13. They were 1.2, 4.7, 9.9,21.5, 37.5, 44.9, 90.9, 179.5, 247.8, 319.2, 429.3, 685.1 and 995 ohms [13]**.** Next is the plotting of velocity coherence plots and frequency response function for all the 13 resistive loads. The substrate material (brass) is assumed to have a young's modulus of 105 GPa and a mass density of 9000 kg/m3. Young's modulus of 3 GPa is assumed (which is much less than Young's moduli of the piezoceramic and substrate) in the bending stiffness (YI) calculations. The total mass per length of the MFC and the bonding epoxy layer are extracted experimentally as 0.0123 kg/m. The laser vibrometer measures the velocity response at Lm= 74 mm. With this MFC sample, the correction factors of the analytical model described in the second section are identified as α= 0.2 and β= 0.5 [13]. The voltage output–to–base acceleration FRF and the relative displacement–to–base acceleration FRF can be removed from the two previously derived equations (35) & (36).

$$v(t) = \frac{\sum_{r=1}^{\infty} \frac{j\omega\kappa_r F_r}{\omega_r^2 - \omega^2 + j^2\zeta_r\omega_r\omega}}{\frac{1}{R_l} + j\omega C_p + \sum_{r=1}^{\infty} \frac{j\omega\kappa_r x_r}{\omega_r^2 - \omega^2 + j^2\zeta_r\omega_r\omega}} e^{j\omega t} \qquad \mathbf{(35)}$$

&

$$W_{rel}(x,t) = \sum_{r=1}^{\infty} [(F_r - x_r \frac{\sum_{r=1}^{\infty} \frac{j\omega\kappa_r F_r}{\omega_r^2 - \omega^2 + j^2\zeta_r\omega_r\omega}}{\frac{1}{R_l} + j\omega C_p + \sum_{r=1}^{\infty} \frac{j\omega\kappa_r x_r}{\omega_r^2 - \omega^2 + j^2\zeta_r\omega_r\omega}}) \frac{\phi_r(x) e^{j\omega t}}{\omega_r^2 - \omega^2 + j^2\zeta_r\omega_r\omega}] \qquad \mathbf{(36)}$$

Some of the geometric parameters for the MFC Unimorph obtained from literature reviews are shown in a table below [13].

Total overhang length, L [mm]	80.5
Overhang length of the active region, L_{act} [mm]	73
Width of the substrate, b_s [mm]	16
Width of the active region, b_{act} [mm]	7.3
Thickness of each piezoceramic fiber, h_p [mm]	0.18
Width of each piezoceramic fiber, b_p [mm]	0.355
Number of piezoceramic fiber, N_p	18
Electrode width in the length direction, u_e [mm]	0.097
Electrode spacing in the length direction, u_0 [mm]	0.41
Effective electrode spacing, Δ_{el} [mm]	0.046
Number of electrode pairs, N_e	72
Thickness of each Kapton layer (in the active region) , h_{ka} [mm]	0.06
Thickness of the Kapton in the inactive region, h_{ki} [mm]	0.12
Thickness of the substrate, h_s [mm]	0.0762
Thickness of the epoxy layer, h_{ep} [mm]	0.028

Table 3.8. Geometric parameters of the MFC Unimorph [13]

3.9 Effect of Substrate Material & Thickness on Piezoelectric Energy Harvesting:

For the second part of the experimental setup**,** the intention was to determine the effect of substrate material and their thickness on piezoelectric energy harvesting from macro fiber composites. For the experimental setup, on the other hand, a set of MFC uni-morphs with several substrate materials and various thicknesses is tested and modelled in this section to investigate the variation of the electrical power output with substrate material and thickness. The same MFC types (M 8507 P1) were selected like the first experimental setup discussed in section (3.7).

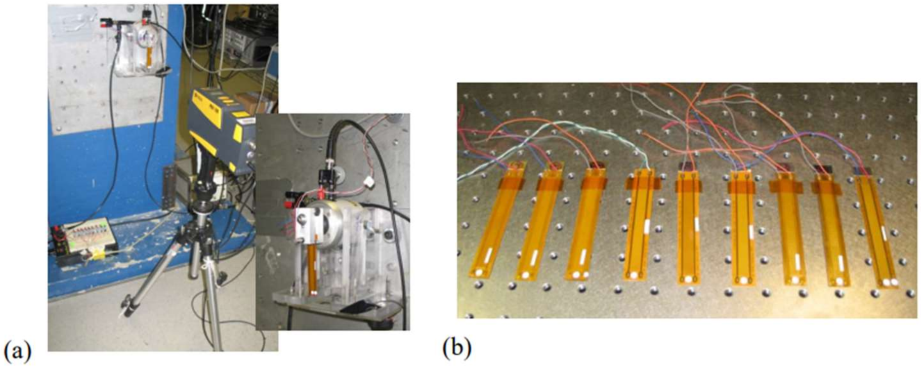

Fig 3.9. Experimental setup for testing Macro Fiber Composites (MFC) unimorph (b) MFC unimorph is attached with three different types of substrates [13]

An experimental setup for MFC with three different substrates with various thicknesses is shown in Figures 3.8 (a) & (b). In the literature review [13], three types of substrates materials, **i.e.** brass, aluminum and stainless steel with three different thicknesses of substrates (0.002", 0.003" and 0.004") [13]. The overhanging length for each of these unimorph is approximately 80 mm. All other relevant information and geometric parameters are provided in Table 1. However, as the experimental data obtained from the literature review [13], the thickness of epoxy and substrate materials are given below in table 2 [13].

Three substrates material (brass, aluminum, and steel) were utilized for this experimental investigation, but for our investigation, we will use completely three different substrates for the first time in the existing knowledge in this arena.

Substrate Materials	Substrate Materials Thickness	Epoxy Average Thickness
Brass	0.0508	0.010
Brass	0.0762	0.028
Brass	0.1016	0.033
Aluminum	0.0508	0.015
Aluminum	0.0762	0.018
Aluminum	01016	0.019
Steel	0.0508	0.020
Steel	0.0762	0.018
Steel	0.1016	0.059

Table 3.9. Different substrate materials with thickness [13]

3.10 Wing Morphing Design for Energy Harvesting

As to the third part of the investigation, the intention was to harvest energy from a flow excited aerofoil/wing. The illustrated experimental setup is shown in figure 3.9 below for performing this investigation. The airfoil (133 mm span and 127 mm chord) is a bimorph with four M 8557 P1 MFC piezo ceramic patches (two on the top surface and two on the bottom surface) [13]. This study employs only the two patches on the top surface for power generation. The electrical outputs of the two MFC patches are combined in parallel and connected to a resistive electrical load. The substrate material for this experiment with the aerofoil was stainless steel.

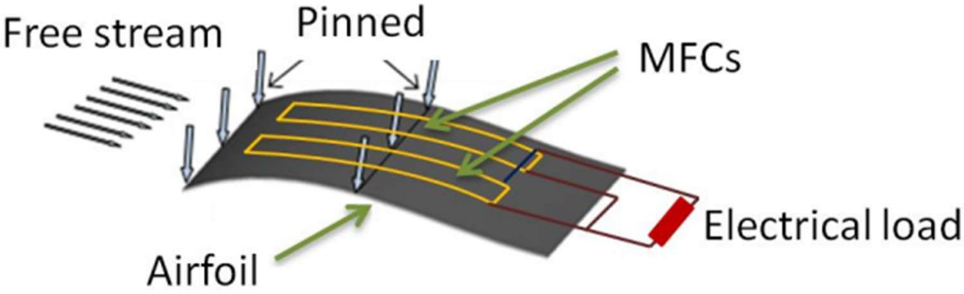

Fig 3.10. Piezoelectric energy harvesting by the flow excitation of a morphing aerofoil [13]

Two MFC patches are placed on the top surface of the aerofoil with two revolute joints, and the position of these two joints were 5% and 10% of the chord from the leading edge of the aerofoil for both patches. The performance of the energy harvesting experiment with the morphing wing/aerofoil resulted to 9.76, 21.2, 52.5, 89.5, 106.9, 320, 494, 661.5 and 995 ohms. For the wind tunnel testing in the literature review [13], the aerofoil was placed in a test section spanwise 137 mm tall and 356 mm wide. The analysis' velocity range was 0 m/s to 15 m/s with a 5 m/s interval, and the angle of attack range was 0° to 30 ° with a 10° interval. The trailing edge velocity of the tested morphing aerofoil and the total voltage output obtained from the experimented MFC patches were measured by using a laser vibrometer. SigLab data acquisition system was used for taking the velocity and voltage signals.

3.11 Macro Fiber Composites for Wing Morphing Design

In the earlier section (3.9), we discussed the energy harvesting technique from the macro fiber composites (MFC) by the flow excitation technique from a thin aerofoil section. However, in this section 3.10, we will focus on instead of using MFC as an energy harvester how we can use them as an actuator to change the shape of the aerofoil to enhance the aerodynamics performance. So earlier, we induced the flow to pass over the aerofoil. We produced the electrical energy from that flow-induced vibration, which could be a potential source of power for aircraft/UAV inflight low power accessories or for feeding the onboard structural health monitoring unit/system. However, here we are doing the opposite; we will apply the electric voltage externally, which will deform the shape of the MFC. As the MFC is attached to the aerofoil, it will change the aerofoil's upper and lower surface shape and improve the aerofoil's performance as per requirement.

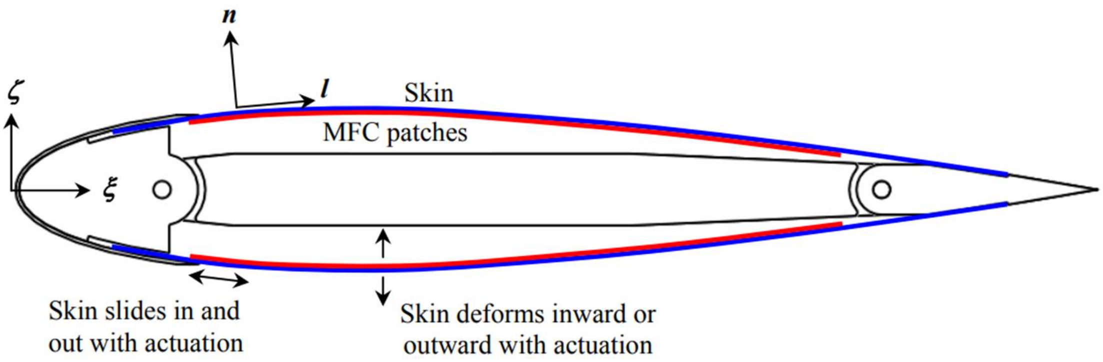

Fig 3.11 (a) Aerofoil Modeled with MFC at both upper and lower surface [19]

For the experimental setup, the modification of symmetric NACA 0015 is essential. The chord length of the modified NACA 0015 aerofoil was 150 mm, and it has a span of 158 mm. However, its shape geometrical properties came close to the NACA 0014 aerofoil after the modification. The upper and lower skin of the experimented aerofoil used a carbon fiber sheet of 0.25 mm thickness.

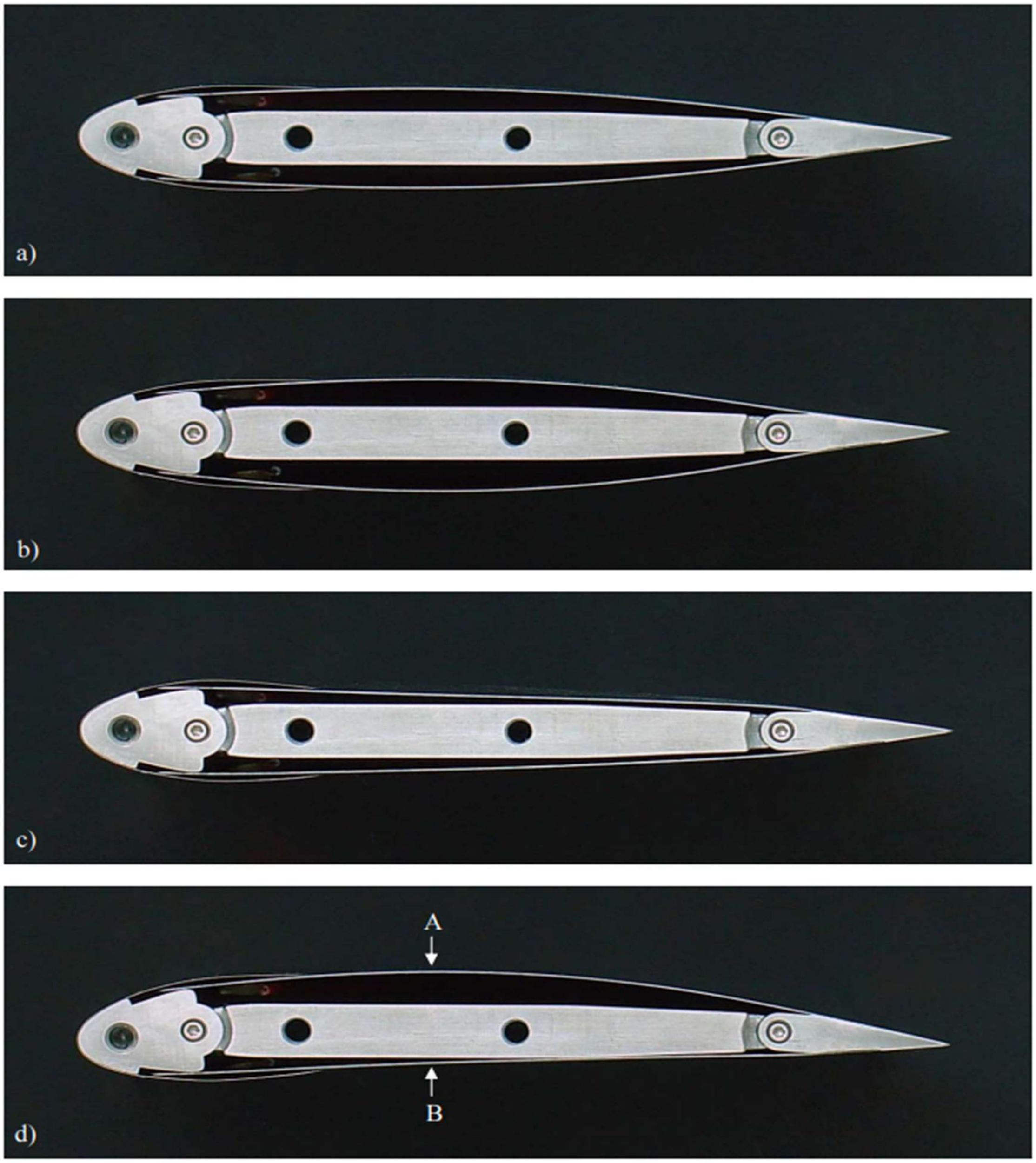

Fig 3.11 (b) Lateral view of the airfoil model: a) without actuation (shape similar to a NACA 0014 airfoil); b) with actuation of both the upper and lower skins at -500 V (shape similar to a NACA 0016 airfoil); c) with actuation of both the upper and lower skins at 1500 V (flatter shape); d) with upper-skin

MFC patches (Smart Material M-8557-PI) are used in the inner side of the aerofoil skin with the help of a vacuum bag. The skin of the aerofoil deformed in the inward direction while a positive voltage was applied simultaneously; the aerofoil deformed in the outward direction when a negative voltage was applied. The movement/deformation of the MFC actuators is performed by HVA 1500/50-2 high-voltage amplifier. The modified aerofoil aerodynamics performance was tested in a small, open-loop, subsonic wind tunnel. Then, this wind tunnel subsonic freestream velocity range was from 0 m/s to 35 m/s**.** The turbulence intensity level of the wind-tunnel freestream is less than 0.25%. Micro-Epsilon optoNCDT 1710-50 laser displacement sensor was used to measure the deformation of the aerofoil skin [19]. Model aerofoil was mounted on a turntable incorporating a balance. The model angle of attack (α) was mounted with this unit's help precisely. This unit can measure the forces and the moments along three perpendicular axes.

Fig 3.11 (c) (a) Prepared Materials for Model Aerofoil Built (b) aerofoil's inner skin with MFC [19]

CHAPTER 4

COMPUTATIONAL INVESTIGATION

4.1 Unimorph Cantilever Beam Configuration:

A cantilever beam's primary use is for piezoelectric energy harvesting can have three different configurations: unimorph, biomorph, and parallel configurations. At the same time, the experimented beam will have one piezoelectric patch attached to its substate material on one side of the beam, known as unimorph. However, if the structure is like a sandwich shape where the metal substrate is in between the two piezoelectric patches, it is called a biomorph. Parallel biomorph's main difference is that this configuration circuit connection is given in series, and for parallel biomorph, circuit connection is in parallel.

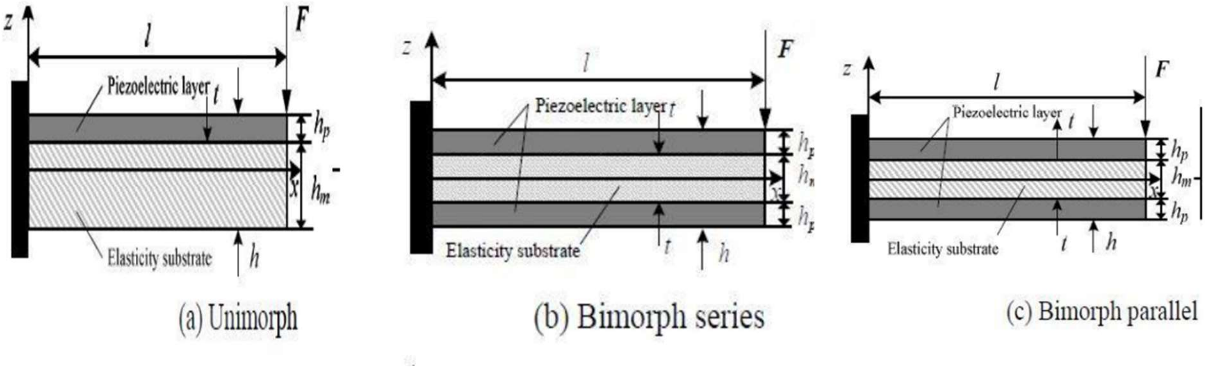

Fig 4.1 (a) Unimorph, biomorph and biomorph parallel configuration [65]

We have chosen the unimorph configuration for the first part of the energy harvesting test by base excitation to compare the energy harvesting analysis with state of art. The resonance frequency is one of the most critical parameters for vibration energy harvesting. The investigation discovered that the power generation density is higher or maximum if the vibration and resonance frequency is matched. Additionally, the piezoelectric harvester's power density decreases when the harvester vibration deviates from its resonance frequency.

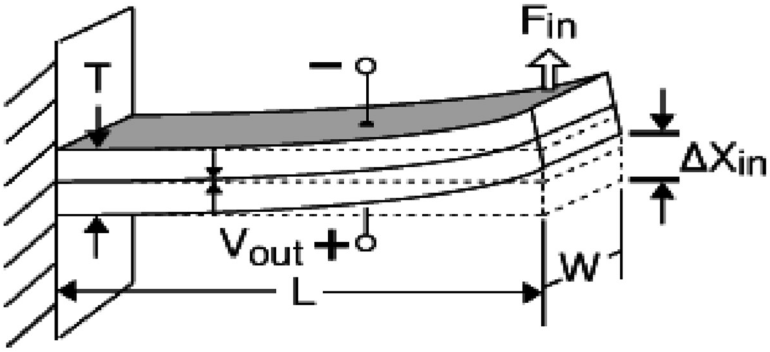

Fig 4.1 (b) Unimorph Cantilever Energy Harvester Configuration [66]

With familiar environmental vibration sources, the vibration frequency range is 60 Hz to 200 Hz, and at the same time**,** acceleration decreases with the generation of a higher mode of frequencies [67]. We used this knowledge when computationally constructing our energy gathered using state-of-the-art experimental data.

4.2 Designing unimorph cantilever beam using ANSYS Workbench:

The mode form of the intended piezoelectric macro fiber composites energy harvester was created and studied using commercially accessible finite element software ANSYS Workbench 2021 R2 student edition. At first, we built the geometric model using the design module of ANSYS Workbench and got the geometric data from state of the art [13] presented in Table 1. The dimension, material selection, and adhesive epoxy were chosen and considered accordingly and made the geometric model in design modeler of ANSYS Workbench to simulate the same environment mentioned in state of the art.

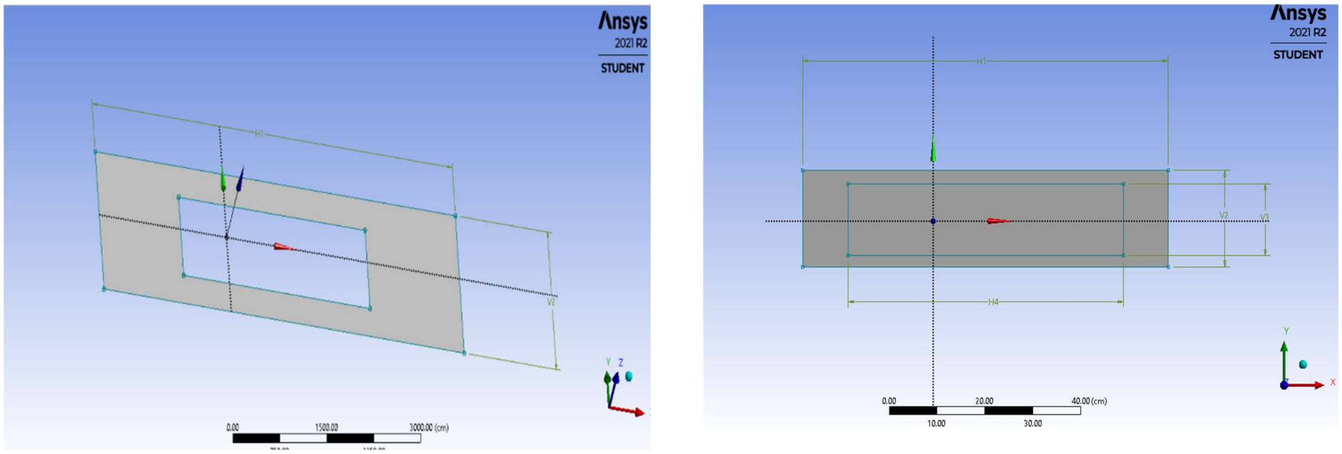

Fig 4.2 (a) Design modeler’s geometry buildup

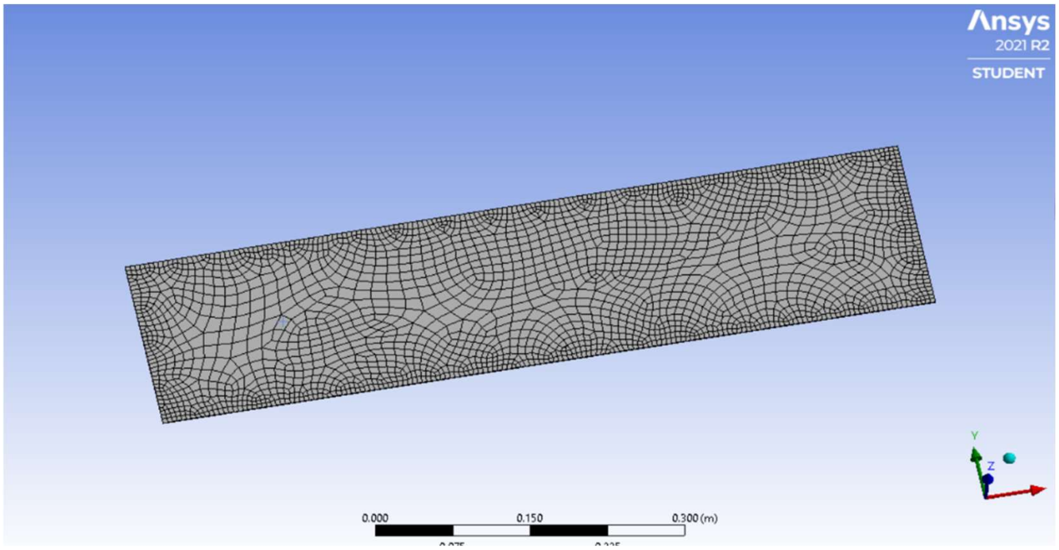

Fig 4.2(b) Model for adaptive meshing

The piezoelectric MFC was placed on top of the metal substrate copper, zinc alloy, and galvanized steel for the geometric design. After completing the geometry in design modular, performing the meshing followed. For meshing purposes, adaptive fine meshing was selected instead of default meshing. After the meshing part, we went through the modal analysis. After defining it as a cantilever and proper boundary condition, the modal analysis was performed. Fixed support was supplied at one end to identify it as a cantilever, while the other end remained free. Then the modal analysis was performed. The six different modal frequencies in Hz are depicted below.

Mode	**Frequency [Hz]**
1	1.4202
2	8.8883
3	11.948
4	24.969
5	36.818
6	49.169

Table 4.2 Six different mode shape for unimorph configuration

For each of these six frequencies, the model form is shown below. The mode shape view defines that the proper boundary layer for a cantilever beam is applied. A fixed boundary condition was placed on the left-hand side of the beam, while the right-hand side or the opposite end was left free. Consequently, there was little distortion on the fixed or left side, as seen in the blue contour.

However, the most significant amount of bending or deformation was seen on the right side, as indicated in the red contour.

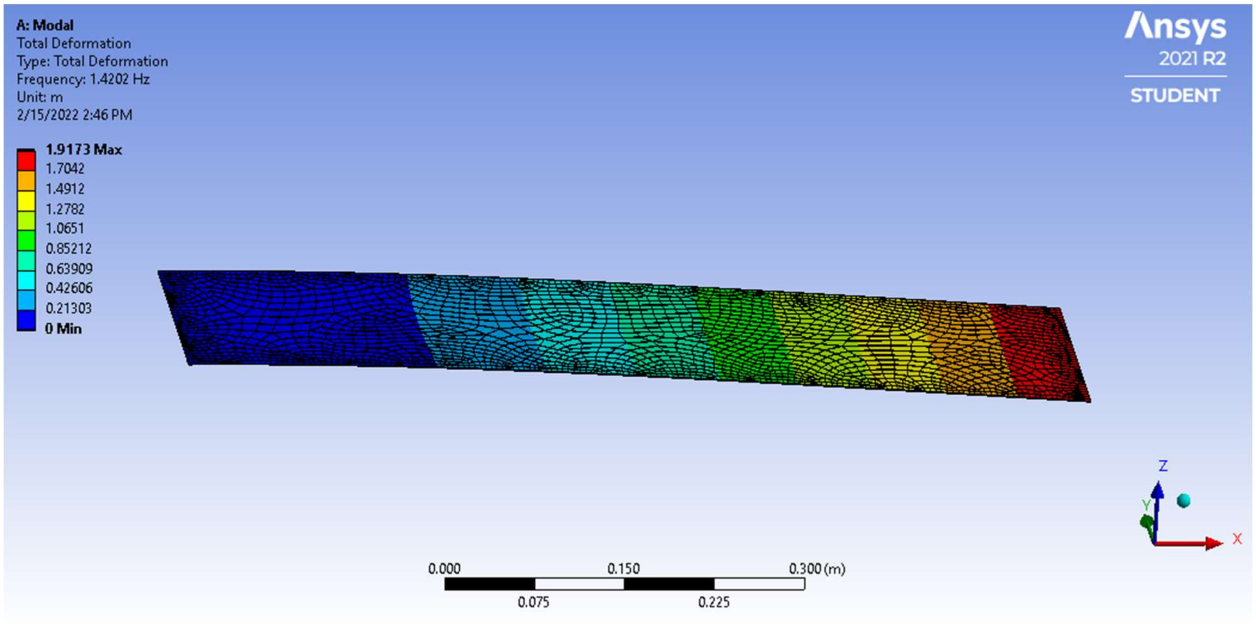

Fig 4.2 (c) Shape of the First Mode

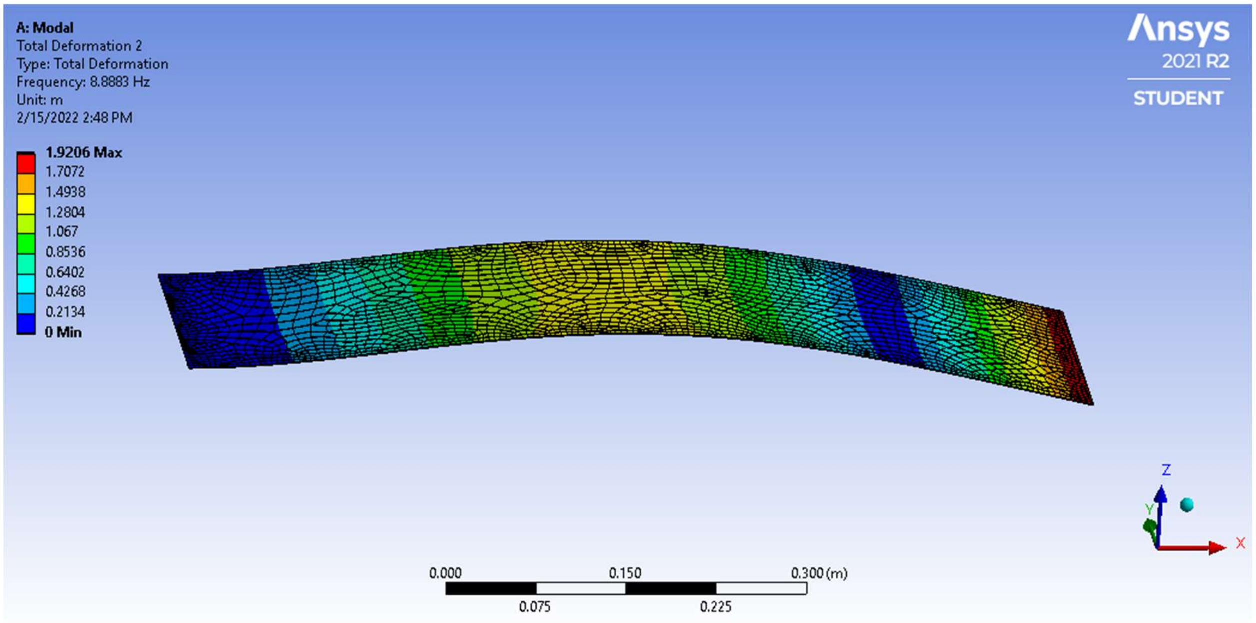

Fig 4.2 (d) Shape of the Second Mode

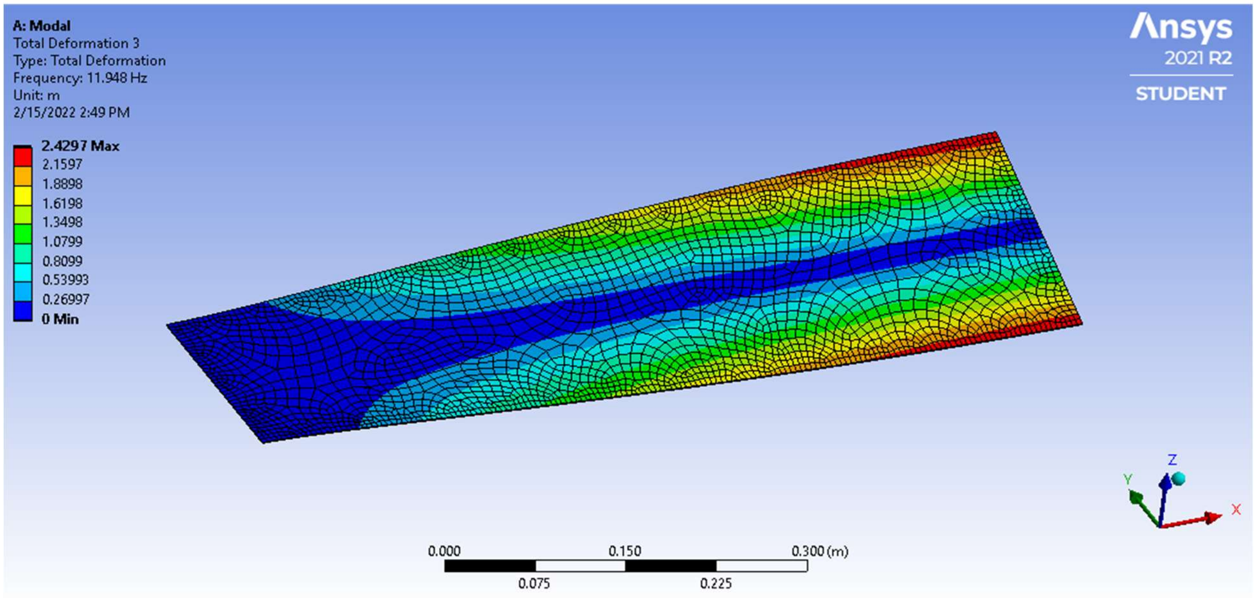

Fig 4.2 (e) Shape of the Third Mode

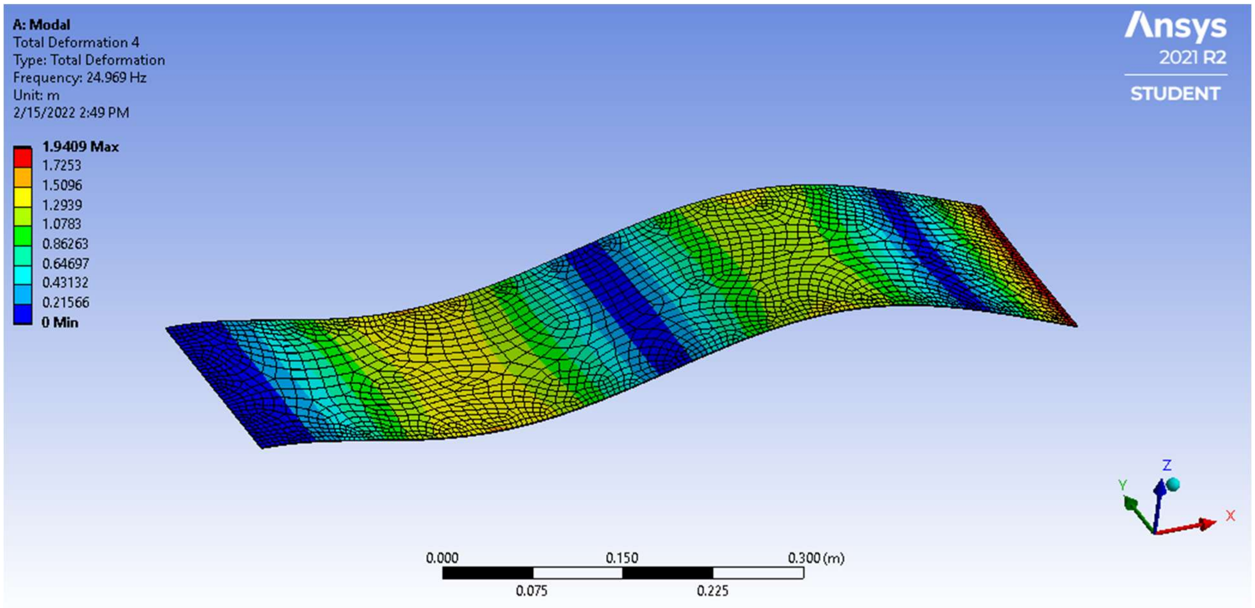

Fig 4.2 (f) Shape of the Fourth Mode

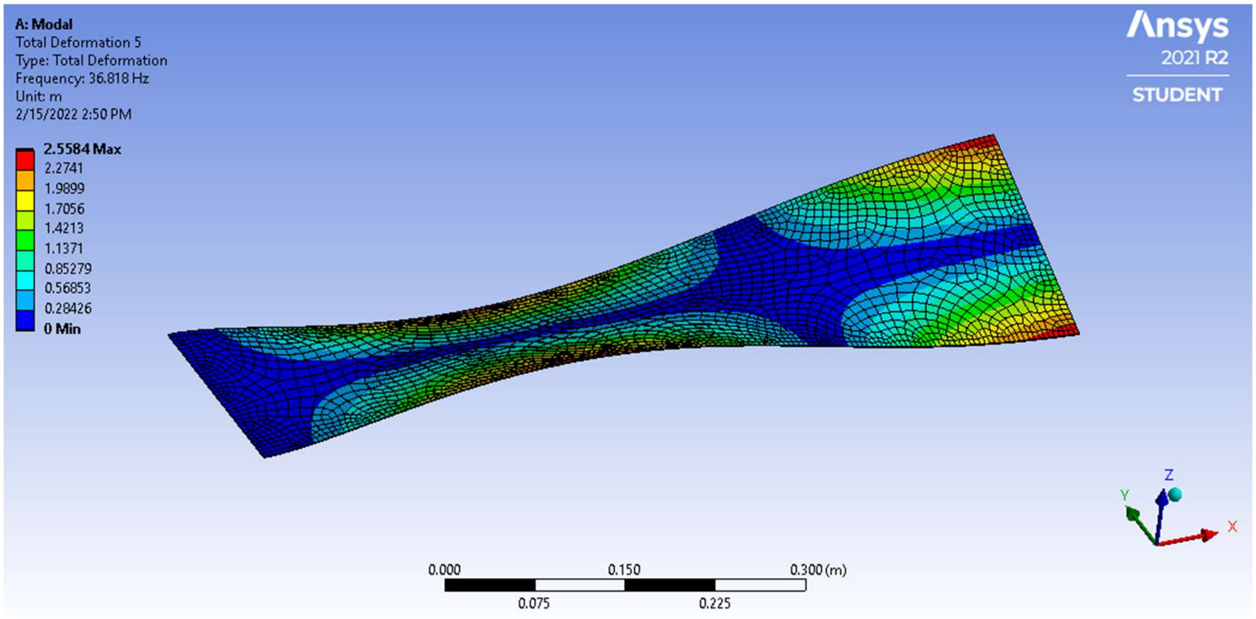

Fig 4.2 (h) Shape of the Fifth Mode

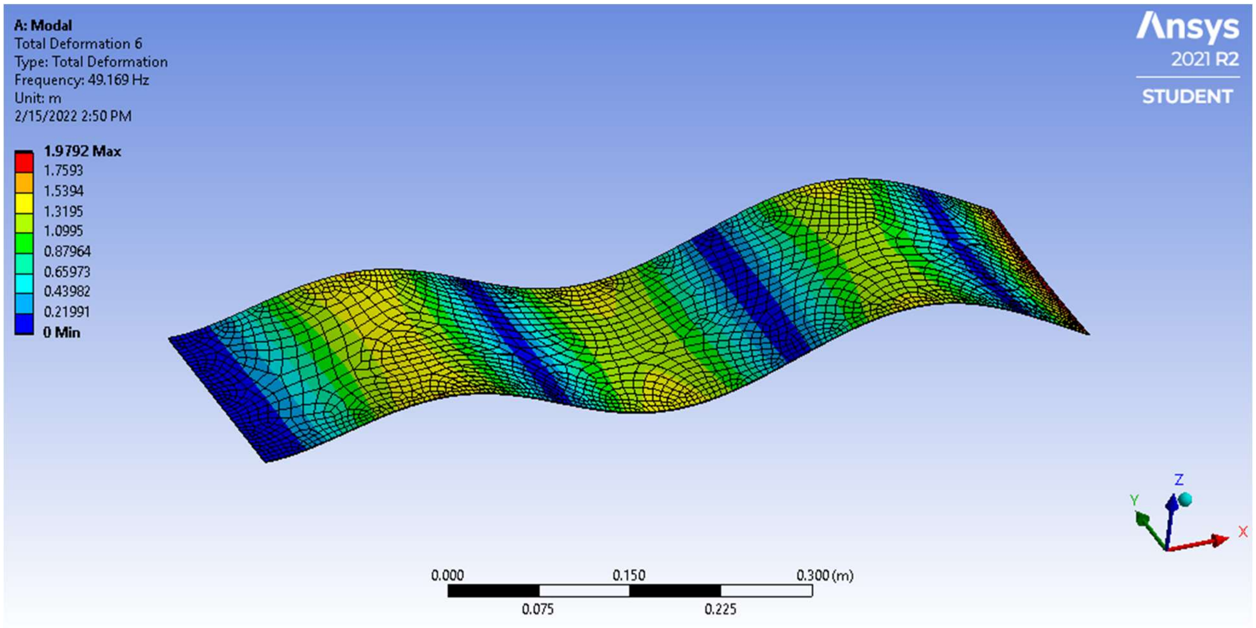

Fig 4.2 (i) Shape of the Sixth Mode

CHAPTER 5

EXPERIMENTAL AND COMPUTATIONAL RESULTS

5.1 Energy harvesting from MFC with different substrates of various thickness

Experimental analysis [13] based on the FRF obtained is shown in the following figure 5.1 using the previously described equation 38. (a). During the experimental examination, natural frequencies were detected.

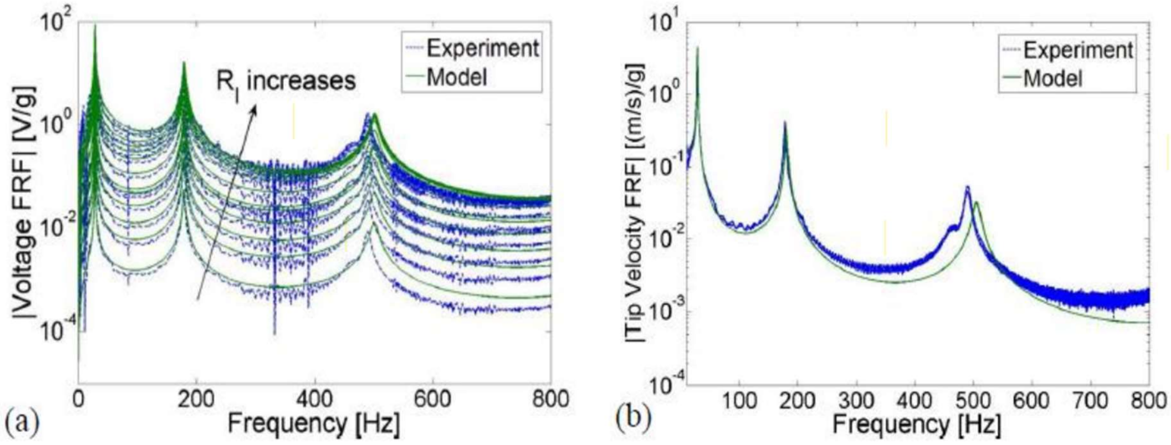

Fig 5.1 (a) Voltage FRF and velocity FRF for different resistive loads (qty. 13) [13]

5.2 Effect of substrate material & thickness

Based on the testing results, the brass substrate was chosen from state of the art to assess the model's correctness. We have added a computational investigation for our analysis by using ANSYS Workbench and applying the same base excitation for the macro fiber composites. The result obtained from the mathematical model, experimental analysis, and our computational investigation is graphically represented in the following figure as peak voltage (V/g) and peak power (mW/g^2) output.

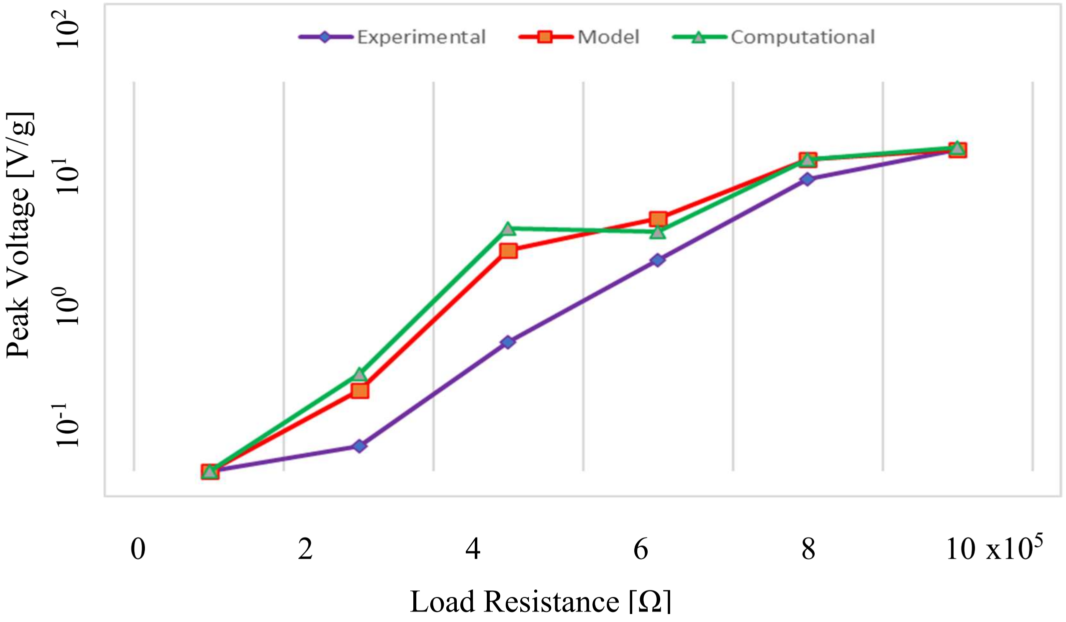

Fig 5.2 (a) Comparison among experimental, model & computational results (peak voltage)

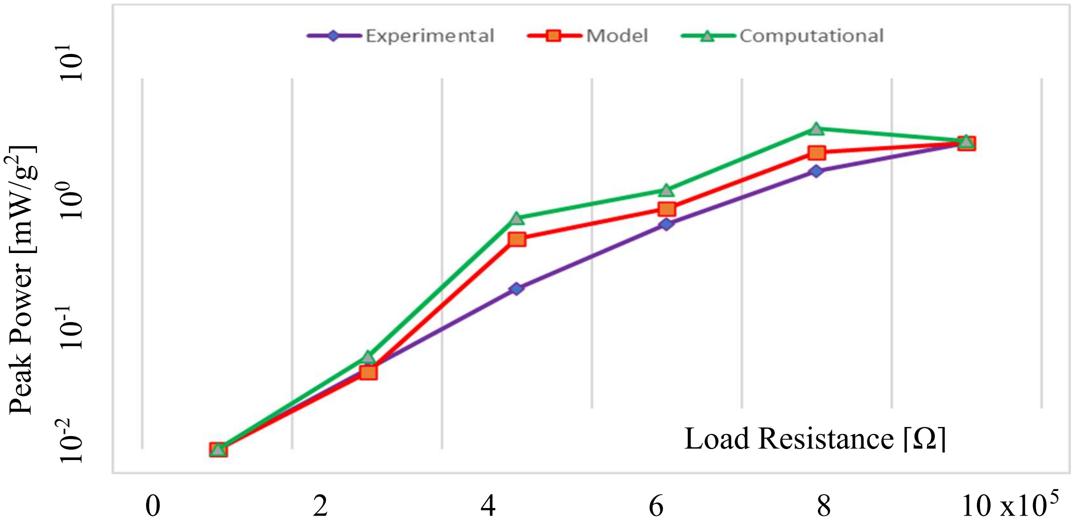

Fig 5.2 (b) Comparison among experimental, model & computational results (peak power)

Our three metal substrates will be evaluated according to their thickness in state of the art [13]. Each substrate material is tested for three different thicknesses of 50.8 µm, 76.2 µm & 101.6 µm. All the parameters used in both design and experiment remained constant in our computational analysis. The copper substrate's most significant peak voltage output was achieved for 50.8 m of thickness for computational analysis, as shown in figures 4.1 (c) and 4.1 (d). However, in this case, the mathematical model built up earlier also provide the second-highest output than the experimental. The same trend was noticed for the power output. Under the same sort of experiment, the highest output was attained from the same thickness of the copper substrate.

For Copper Substrates:

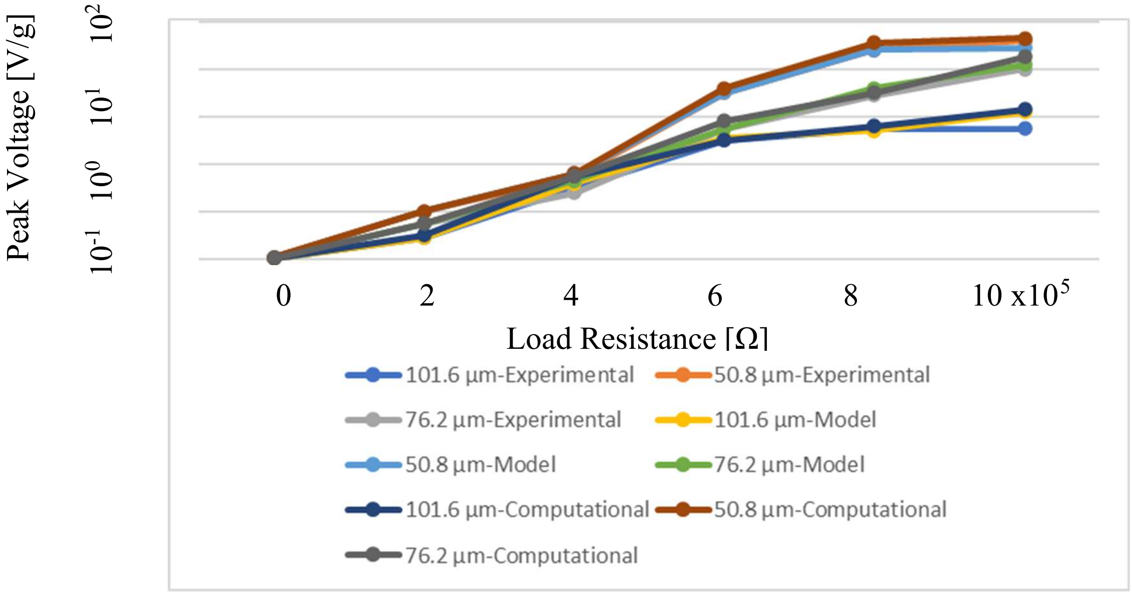

Fig 5.2 (c) Peak voltage's variation for copper substrate for the different thickness

Our second substrate material to be taken into consideration is zinc alloy. For zinc alloy substrate, likewise copper alloy, we have chosen three same thicknesses for better comparison. From Fig 5.2 (d), the peak power variation for a copper substrate for three different thicknesses for both the peak voltage output and peak power output for computational analysis. Here, the mathematical model prediction was more significant than the experimental.

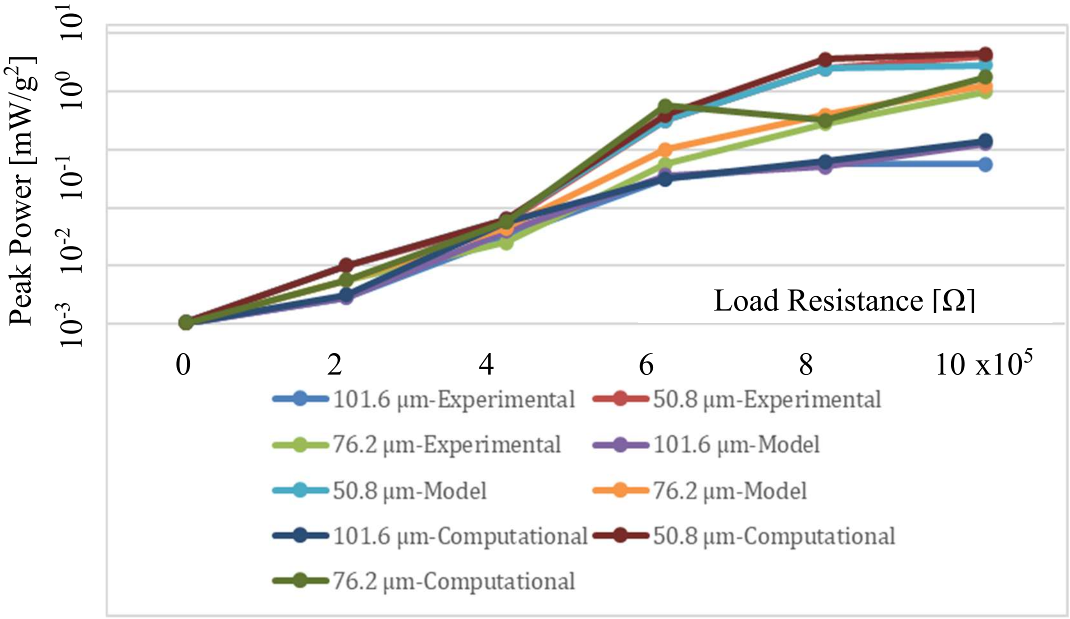

Fig 5.2 (d) Peak power's variation for copper substrate for three different thickness

Zinc Alloy Substrates:

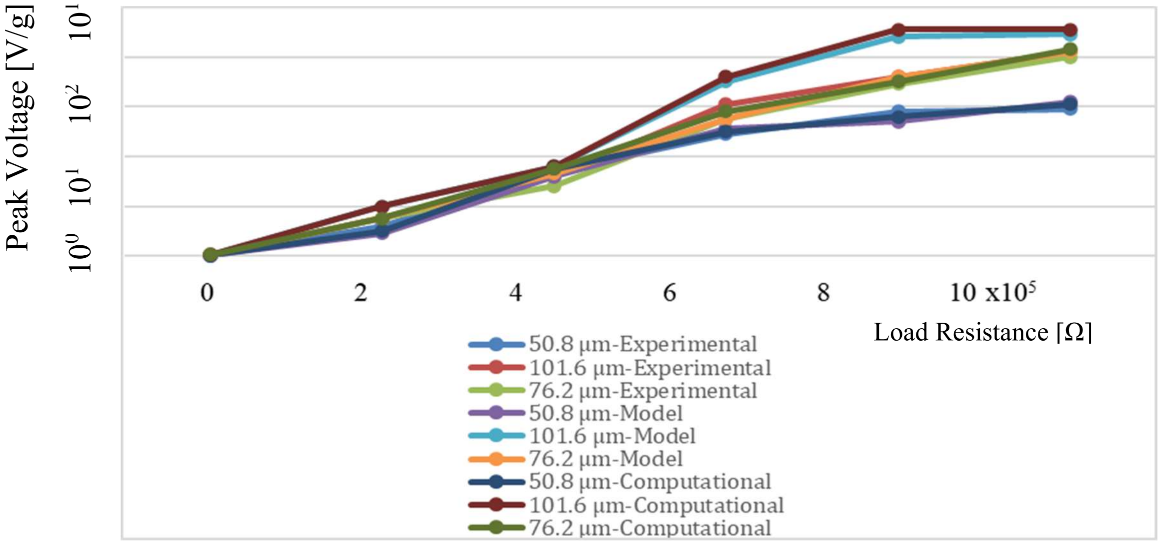

Fig 5.2 (e) Peak voltage's variation for zinc alloy substrate for three different thickness

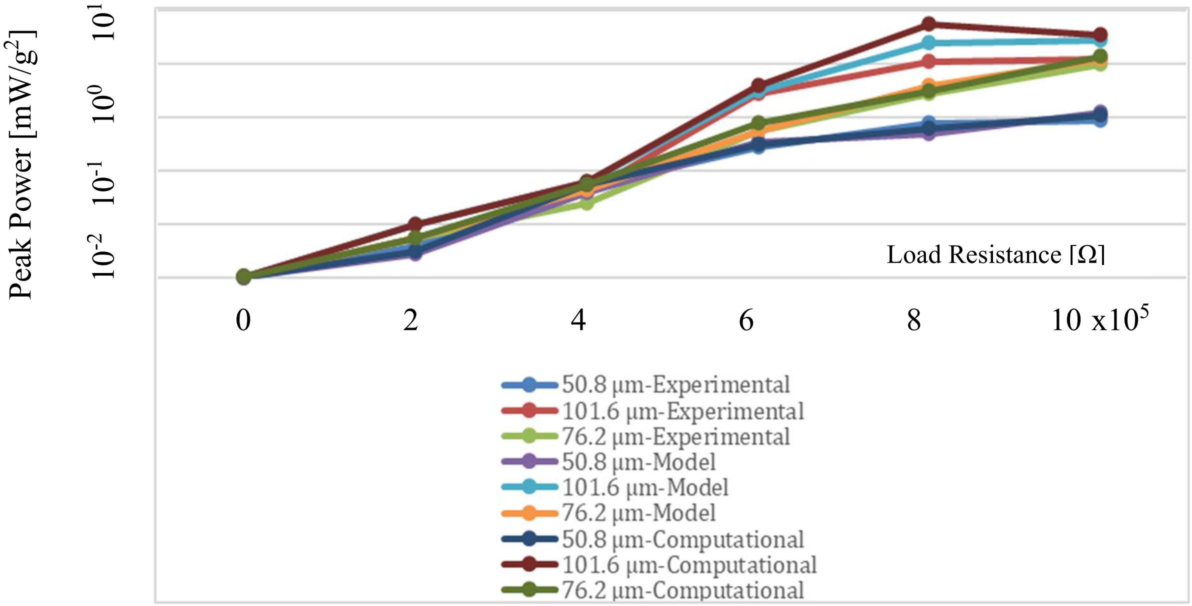

Fig 5.2 (f) Peak power's variation for zinc alloy substrate for three different thickness

Galvanized steel substrates:

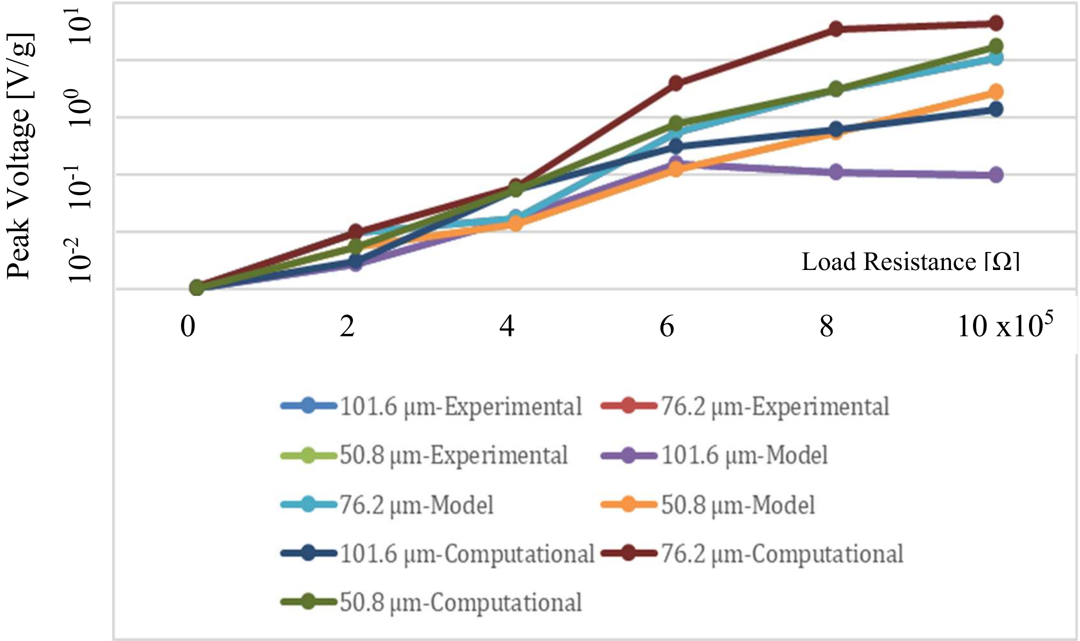

Fig 5.2 (g) Peak voltage's variation for galvanized steel substrate for three different thickness

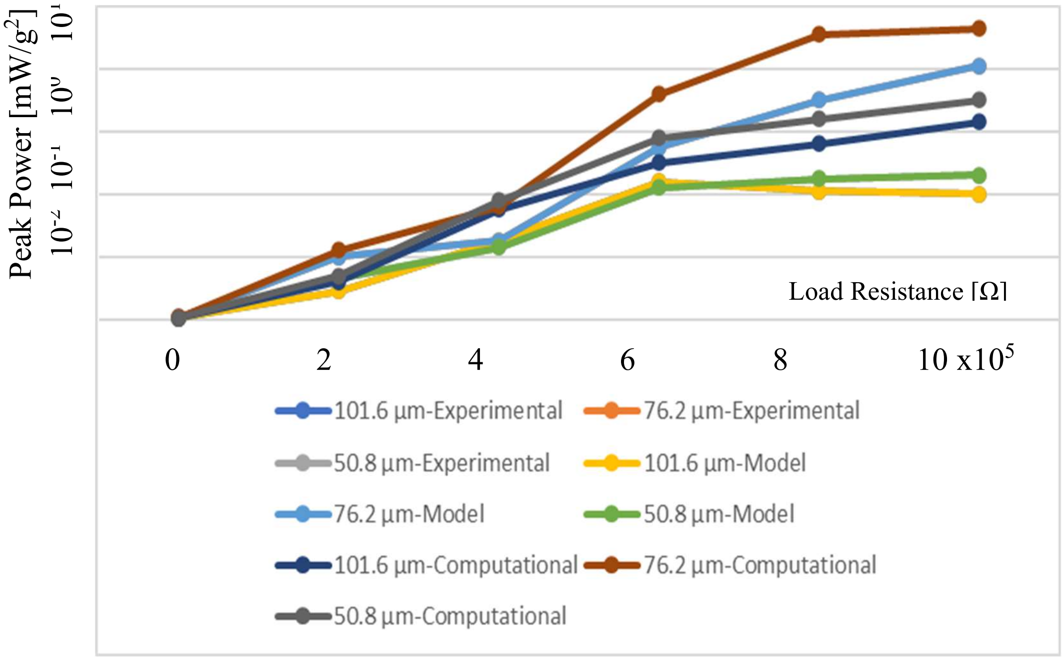

Fig 5.2 (h) Peak voltage's variation for galvanized steel substrate for three different thickness

Figures 4.4 (e) and (f) show that, unlike the copper substrate, the most significant peak voltage output was achieved with a zinc alloy thickness of 101.6 m. This same thickness dominates after analyzing the first two substrates, copper, and zinc alloy, our third and last substrates was galvanized steel. For the computational study approach, 76.2 m thickness of the galvanized substrate with macro fiber composites (MFC) patches generates the most significant peak voltage and peak power production compared to the first two substrates.

Here, the mathematical model also yields slightly more peak voltage and power output than the experimental investigation. Moreover, this trend remains valid for all these three types of substrates. However, our computational approach predicted the highest output in all three cases compared to both experimental and numerical/mathematical models.

5.3 Energy Harvesting Dependency on Types of Substrates (Computational Data):

Accompanying our comparison of these three new substrates for these three thicknesses with MFC patches, we examined these three thicknesses for three substrate materials in terms of peak power production for computational research in the following 5.3 (a) figure. From Figure 5.3 (a), we may deduce that, in a computer study using commercial finite element analysis software, zinc alloy substrates with a thickness of 101.6 m generate the highest peak power output**.** In contrast, galvanized steel with 76.2 m was the closest rival. Though zinc alloy of 101 µm thickness provides maximum output, the difference between zinc alloy and galvanized steel for these two specific thicknesses was much less.

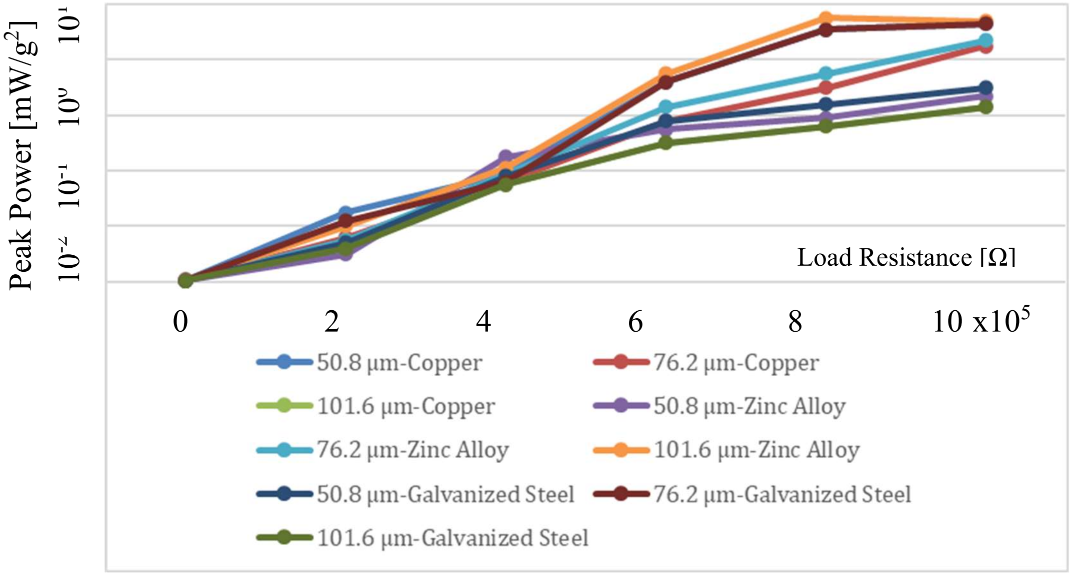

Fig 5.3 (a) peak power's variation for three substrates for three different thickness (computational)

5.4 Energy harvesting from flow excited aerofoil:

For the energy harvesting from an aerofoil excitation, we built a very thin aerofoil by the best

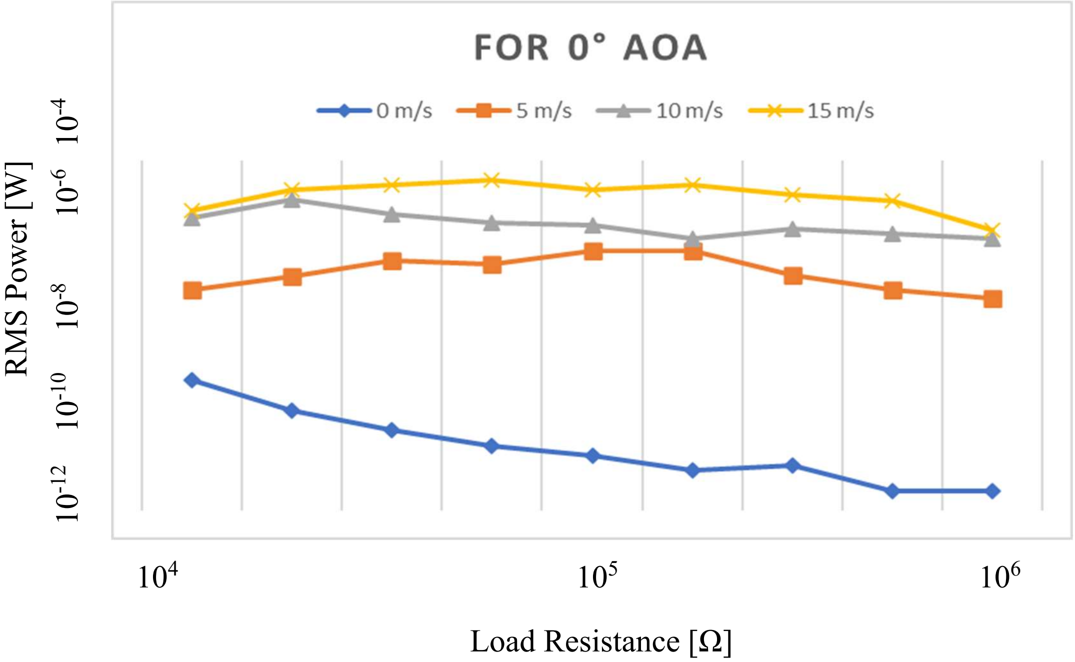

Fig 5.4 (a) RMS Power Output for 0° Angle of Attack

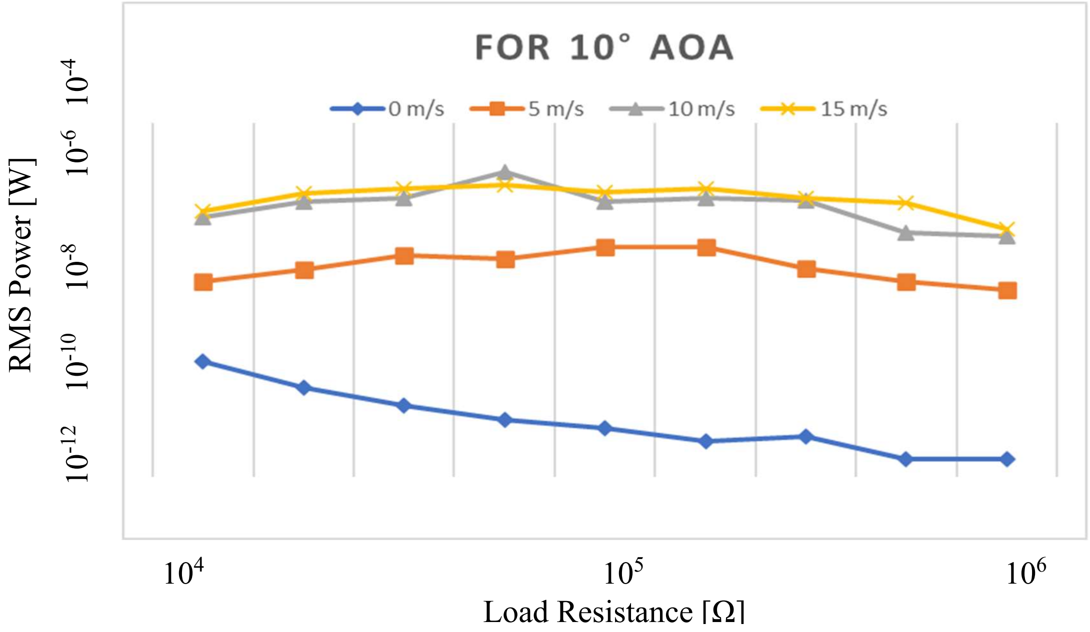

Fig. 5.4 (b) RMS Power Output for 10° Angle of Attack

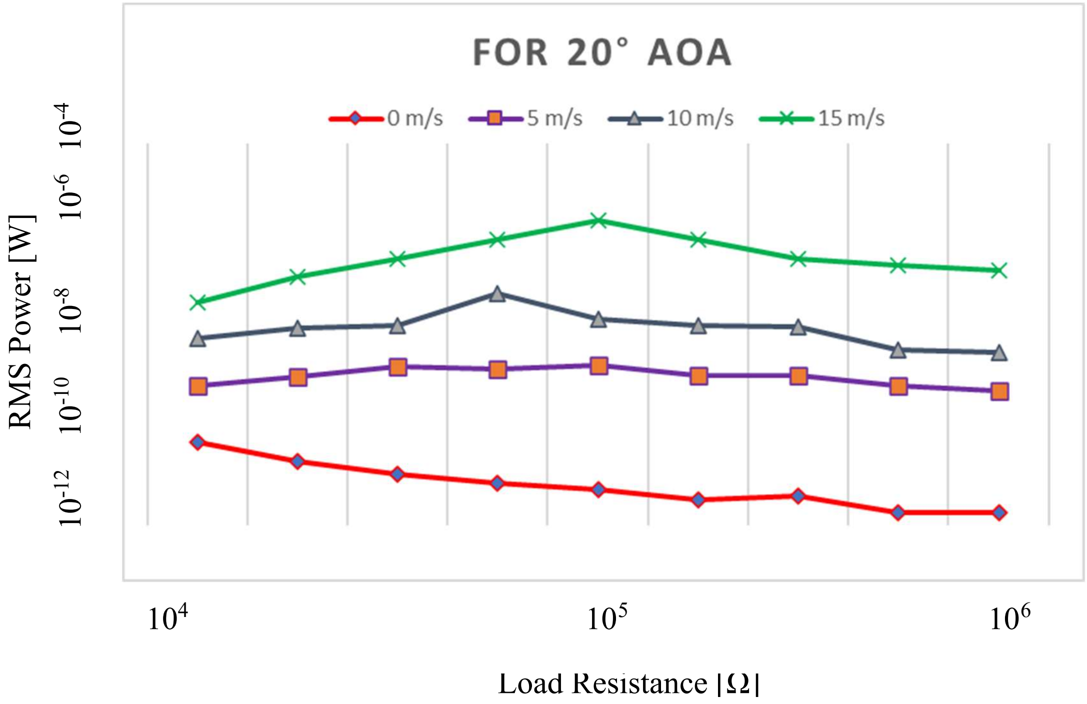

Fig. 5.4 (c) RMS Power Output for 20° Angle of Attack

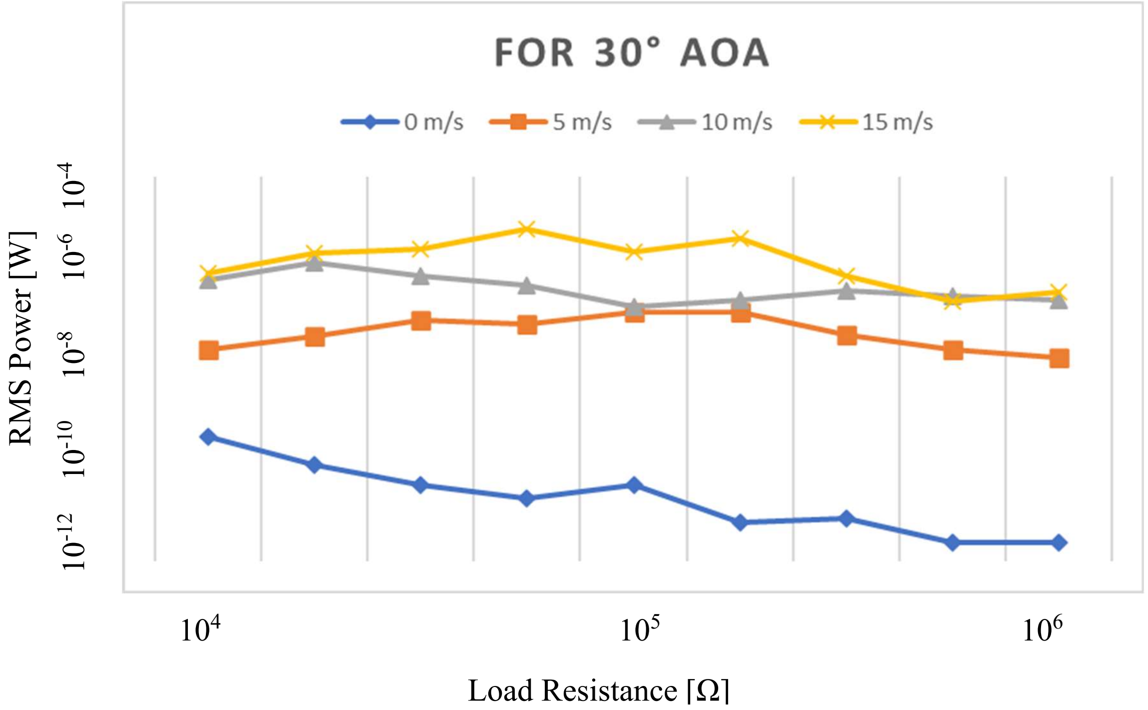

Fig. 5.4 (d) RMS Power Output for 30° Angle of Attack

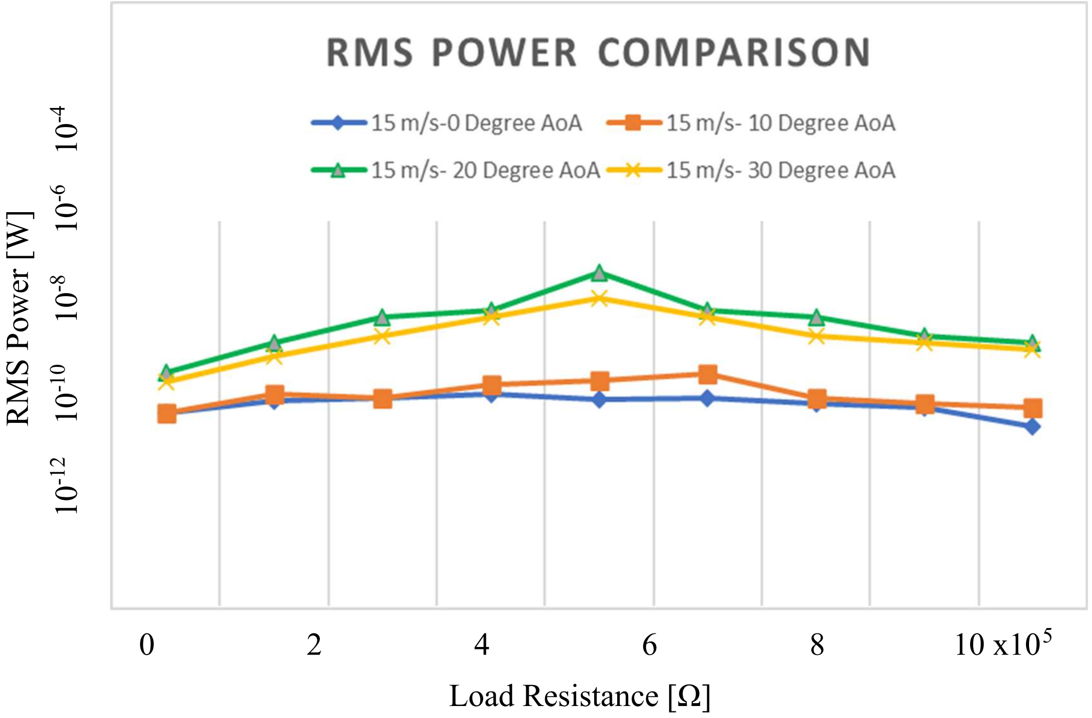

Fig. 5.4 (e) Comparison of RMS Power Output for various Angle of Attack

We have used ANSYS Fluent computational fluid dynamics analysis to conduct this part of the analysis. The idea was to set up or attach the macro fiber composites (MFC) patch to the thin aerofoil's top surface and its substrate material, as shown in figure 3.9 in chapter 3. Four different types of angles of attack (α) were chosen for this test (0), and flow velocity was chosen (0°, 10°, 20° & 30°). The four-velocity/incoming flow velocity to the inlet of the aerofoil (0 m/s, 5 m/s, 10 m/s, and 15 m/s) was chosen.

Fig 5.4 (a) shows that maximum RMS power output was gained as 15 m/s while the angle of attack for the analysis was 0° and the lowest power output was for 0 m/s. Nevertheless, for figure 5.4 (b), though the maximum beginning power was obtained for 15 m/s, it was noticed that for ten m/s highest picks gained happened.

Figure 5.4 (c) for 20° AoA shows that the RMS power output for 15 m/s remained constant throughout the experiment, indicating a significant difference between these flow velocities regimes. Figure 5.4 (d) shows a similar pattern to the previous figure. However, there was not as much difference in power output for ten m/s and 15 m/s at first. With altering load resistance, there was a noticeable power output improvement.

From all these four figures, it is decided that the RMS power output increases with the highest velocity of the fluid/airflow. The reason behind this is straightforward though as the velocity of air increases, the amount of flow-induced vibration also increases. Hence, the MFC patches produce more power from this vibration source.

A combined observation made in figure 5.4 (e) shows that even though the same aerofoil was kept at 15 m/s but for an angle of attack, 20° produces more RMS power output than the 30° angle of attack for given airflow velocity. Based on these four data, it is determined that the RMS power output increases as the fluid/airflow velocity increases. As a result, to design an energy harvesting UAV wing, it is crucial to operating/ fly it through a sufficient airflow velocity (airspeed) and ensure it is precise/suitable angle of attack (α).

5.5 Wing morphing design with MFC actuators

So far, we have employed macro fiber composites (MFC) to harvest energy from vibration sources or base excitation in our research. We attached these MFC patches to thing aerofoil section and its best-suited substrate material and thickness. Then, let the flow pass over it to produce flow-induced vibration to harvest electrical energy that can be useful to feed for UAV or small aircraft different inflight operations, including structural health monitoring. However, for this section of the research, we employ piezoelectric macro fiber composites patches as an actuator to deform (stretch or squeeze) its shape into several forms of aerofoils. For example, from the state of the art, we knew that using an MFC actuator can change the shape of a NACA 0014 aerofoil to NACA 0016 aerofoil [19]. In a real-life scenario, these types of morphing wing applications promise to change the aircraft wing's inflight shape and meet the in-demand flight requirements. We choose the computational fluid dynamics (CFD) approach for our analysis using commercially available CFD software ANSYS Fluent. As mentioned in the literature review, the exact simulation condition was maintained [19]. By applying -550 V, we will try to convert a NACA 0010 symmetric aerofoil to a NACA 0012 aerofoil, perform a CFD simulation of that NACA 0012 aerofoil, and perform a detailed, detailed, and perform a detailed comparative study. Convergence criteria 10-3. One equation Spalart-Almaraz Model was chosen as a turbulence model.

The Y+ value must be smaller than 1.0. The mesh that was taken into account was constructed over the whole domain. It was decided to use a high-quality quadrilateral mesh. The mesh sizing was about 0.05 m, along with proximity and curvature size function. The total number of Nodes was 41687, and the total number of elements was 41266. Plants were created using inflation to capture the boundary layers and flow separation near the airfoil. A total of 10 layers of inflation were created to capture the separation. The layers were chosen with a transition ratio of 0.2 and a growth rate of 1.2 to capture the boundary layer flow and separation. ANSYS Fluent design modeller was used for geometry buildup in fig 5.5 (a). Modified NACA 0010 aerofoil, now equivalent to NACA 0012, is visible inside the fluid domain in slight green color in figure 5.5 (a).

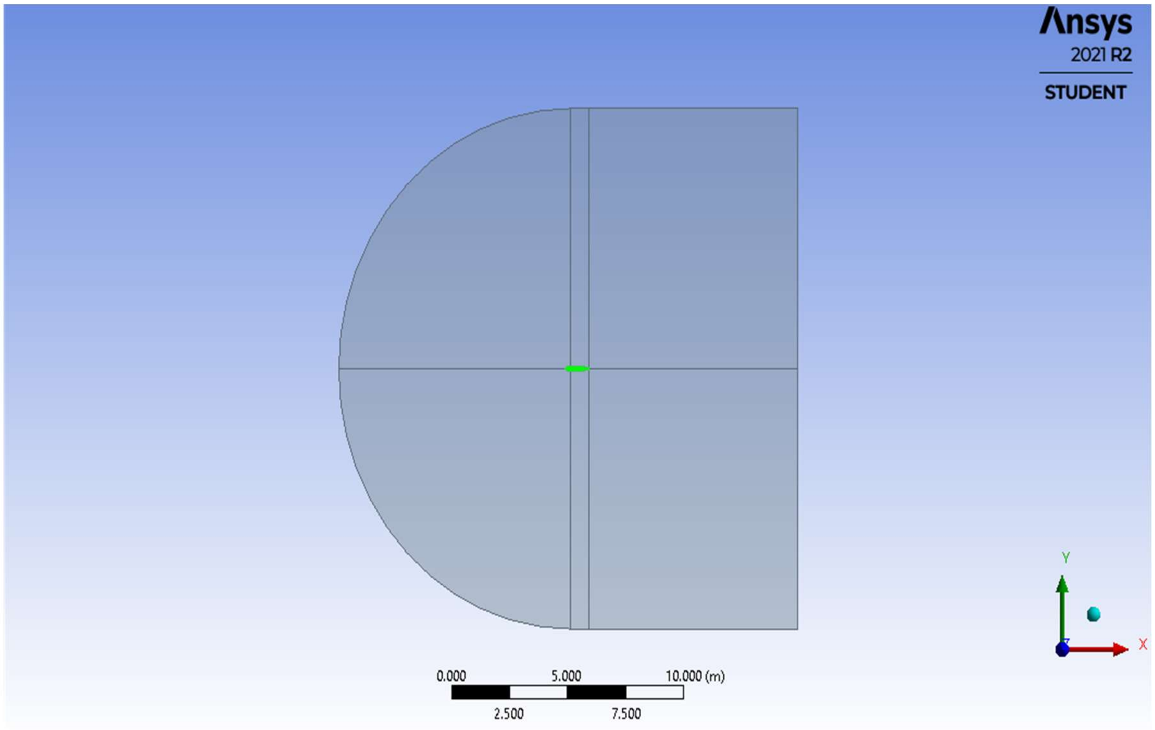

Fig 5.5 (a) Fluid domain-NACA 0012 aerofoil inside (green color)

To reproduce the experimental analysis in fig. 5.5, a renowned "D" shape mesh was created to create a virtual wind tunnel environment (b). The fluid domain was 21 times that of the aerofoil chord length (i.e. 21c). For the simulation purpose, the aerofoil body was defined as "wall", the leading edge of the aerofoil flow domain was "inlet", and the trailing edge portion was "outflow" to simulate a virtual wind tunnel. As shown in figure 5.5, an excellent mesh is built to capture the fluid flow behavior across the aerofoil surface, mainly where MFC patches are employed at the top and bottom of the aerofoil body and where boundary layer creation and separation occur (b).

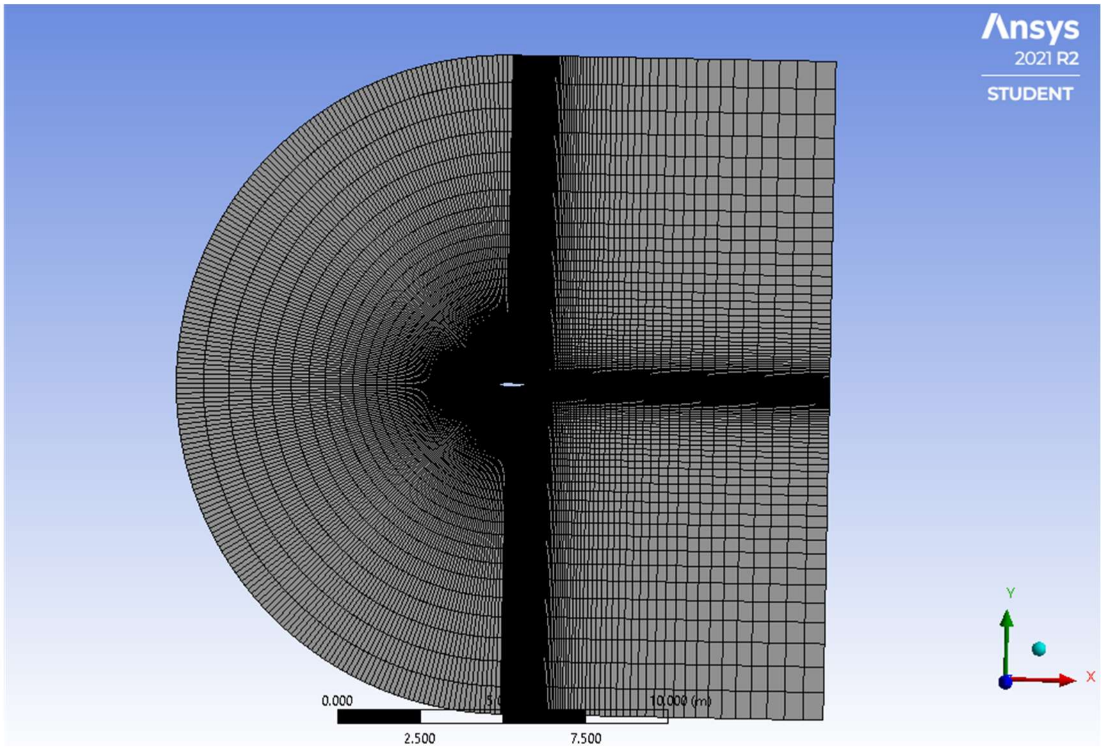

Fig 5.5 (b) Mesh generation for modified NACA 0012 aerofoil (originally NACA 0010) Fine mesh

provides better accuracy of the simulation performed. The number of iterations for each simulation was taken 1000 to reduce the simulation time, and it was found that within this number of iterations solution converged very efficiently. The following figures show the pressure contour, velocity contour with flow direction in both the x and y axes and the velocity vector for the NACA 0012 aerofoil.

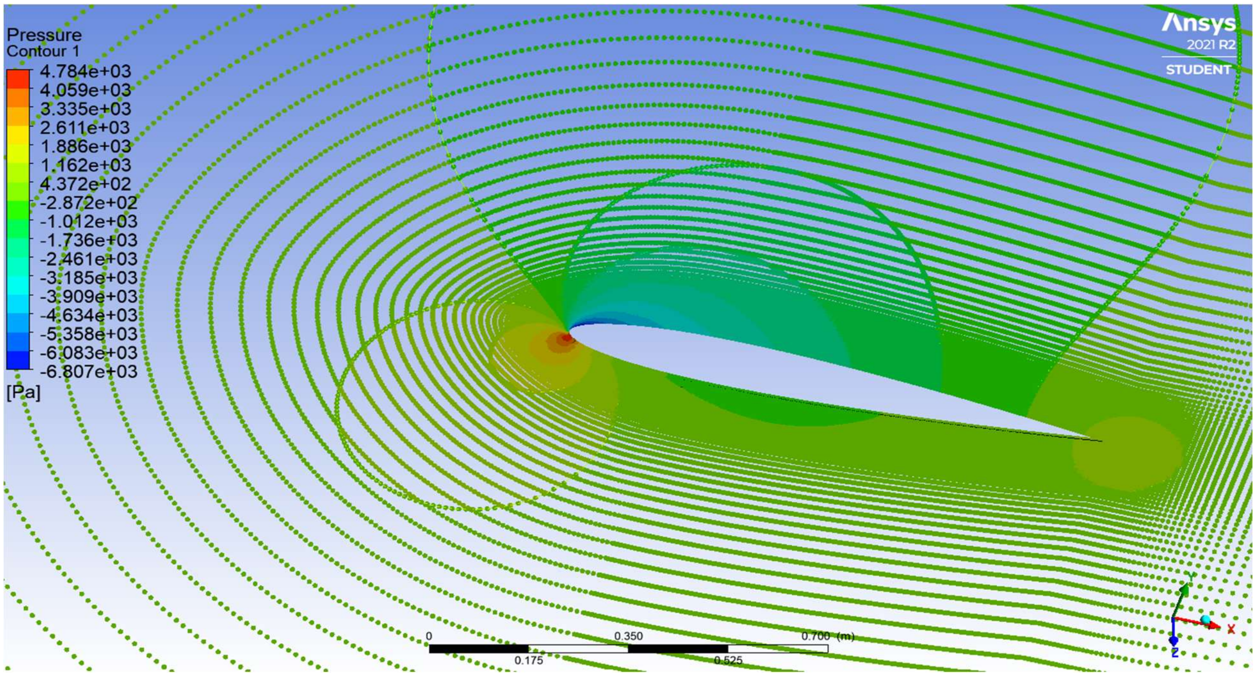

Fig. 5.5 (c) Pressure contour for modified NACA 0012 aerofoil

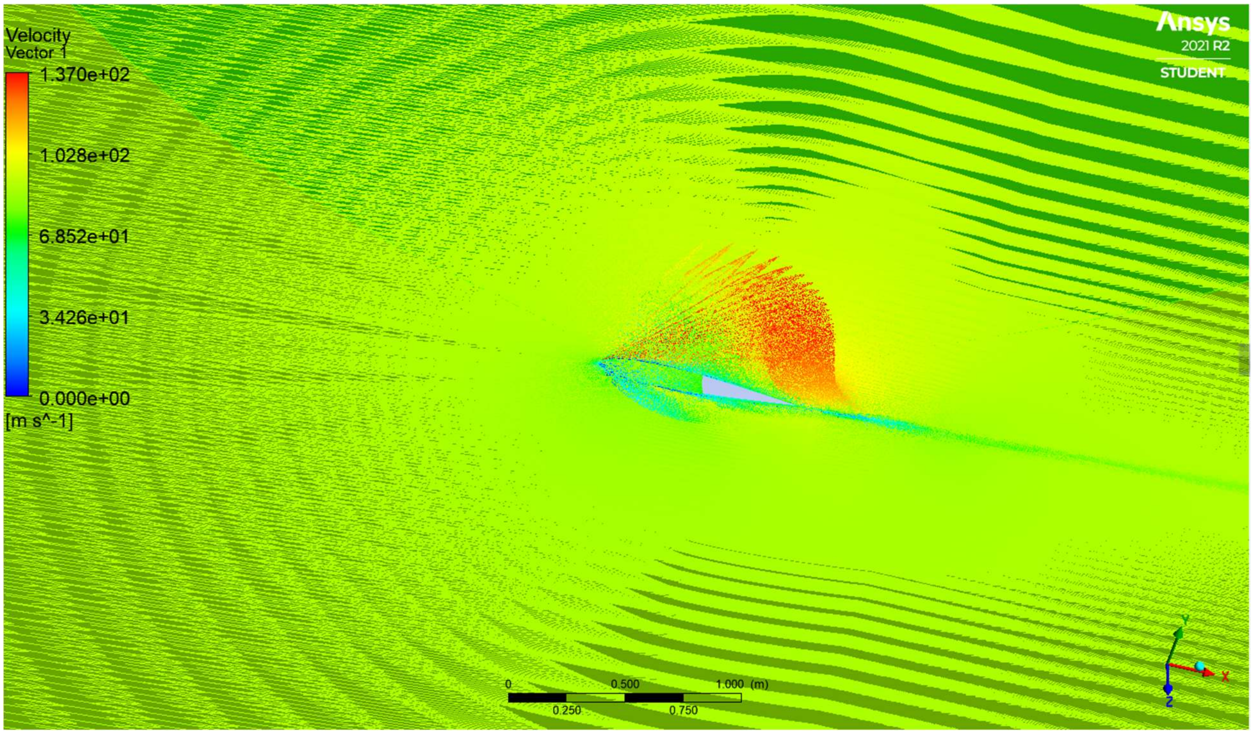

Fig. 5.5 (d) Velocity vector for modified NACA 0012 aerofoil

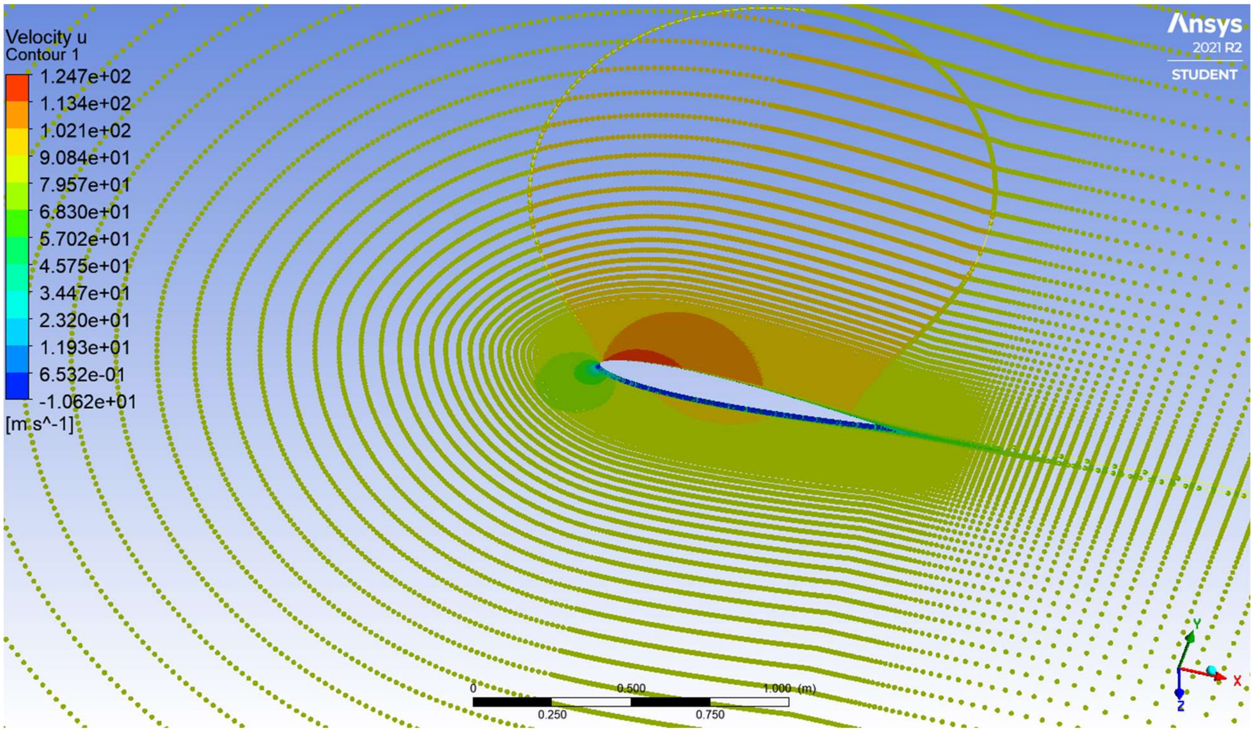

Fig. 5.5 (e) Velocity contour (u) for modified NACA 0012 aerofoil

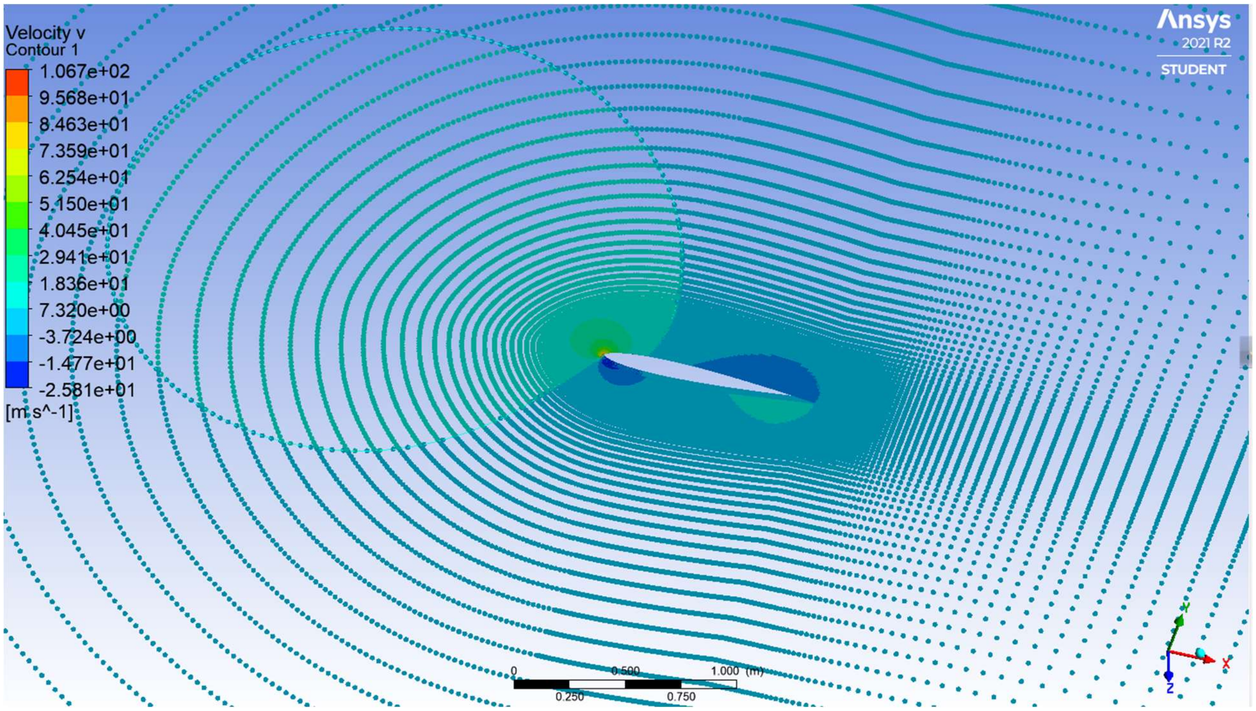

Fig. 5.5 (f) Velocity contour (v) for modified NACA 0012 aerofoil

After completing the computational fluid dynamics (CFD) simulation, the aerodynamics data

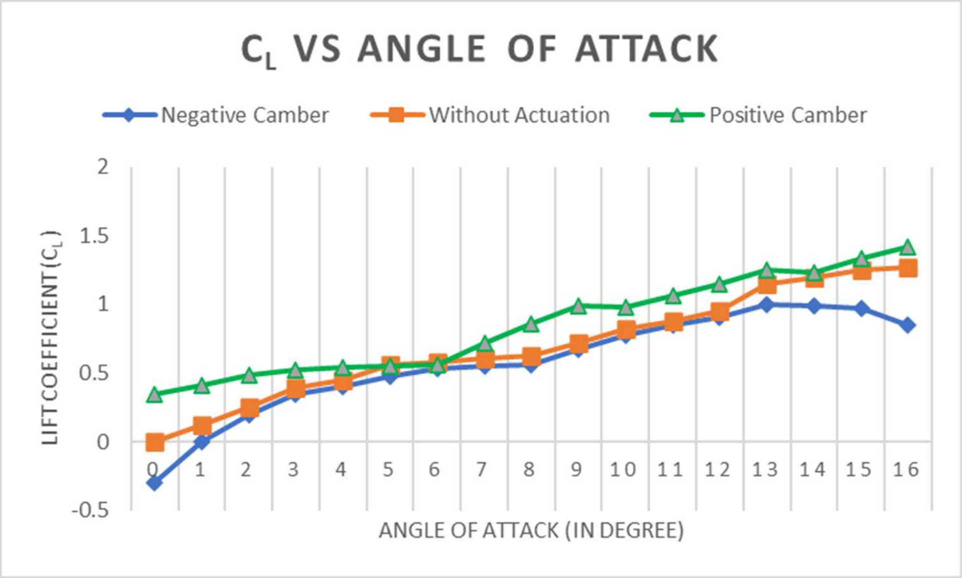

Fig 5.5 (g) Lift coefficient (C_L) vs Angle of Attack (α)

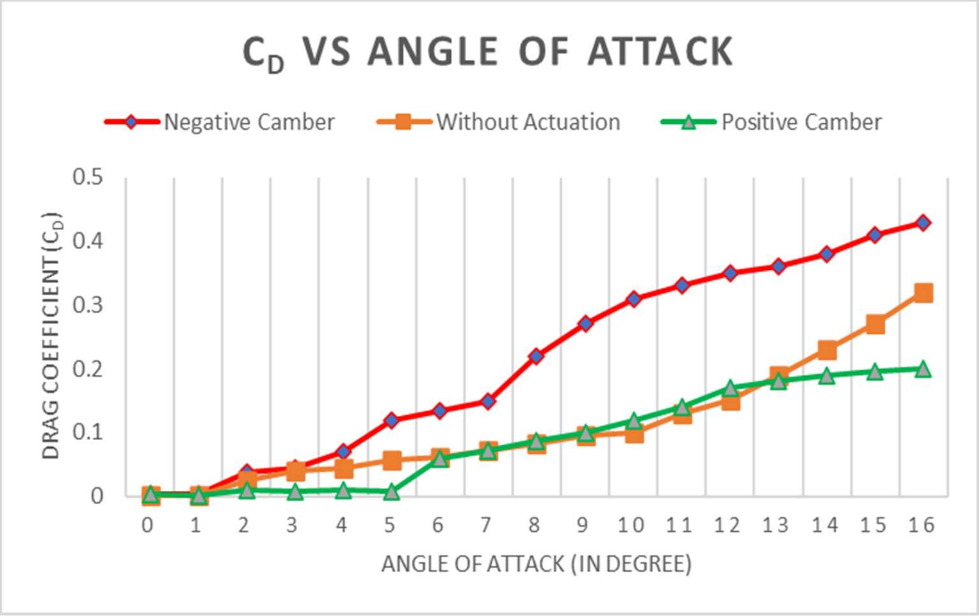

Fig 5.5 (h) Drag coefficient (C_D) vs Angle of Attack (α)

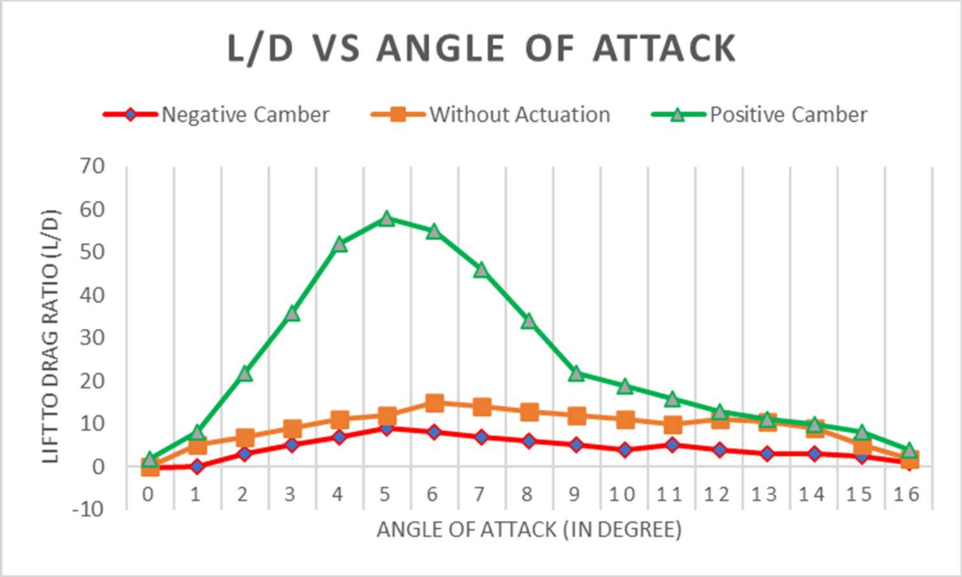

Fig 5.5 (i) Lift to Drag ratio (L/D) vs Angle of Attack (α)

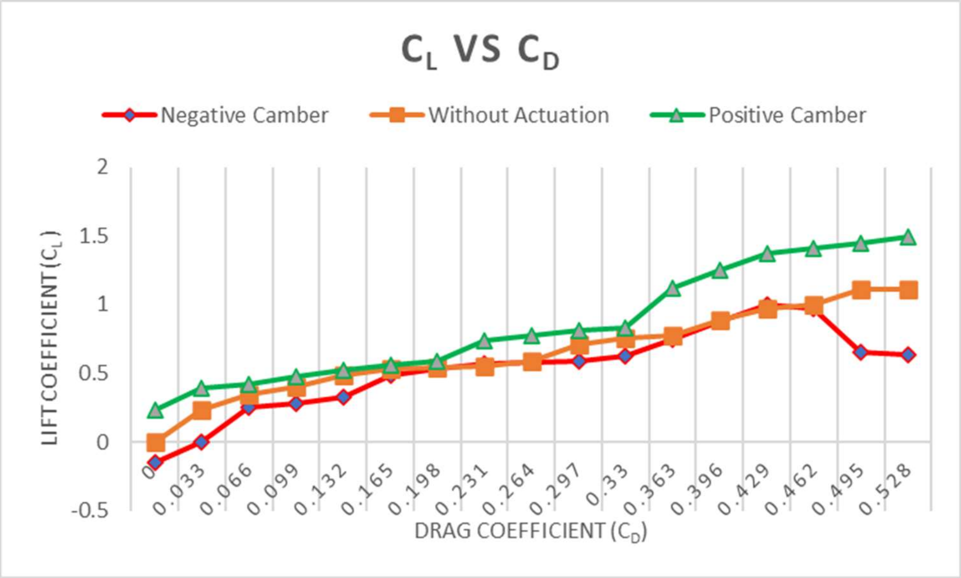

Fig 5.5 (j) Lift coefficient (C_L) vs Drag coefficient (C_D)

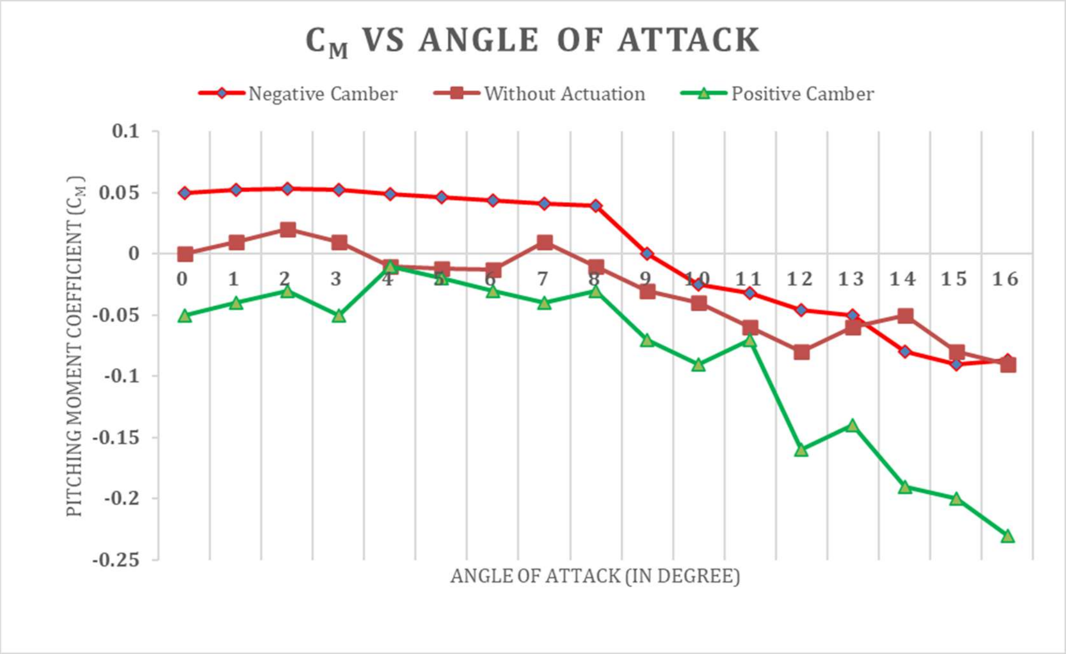

Fig 5.5 (k) Pitching moment coefficient (C_M) vs Angle of Attack (α)

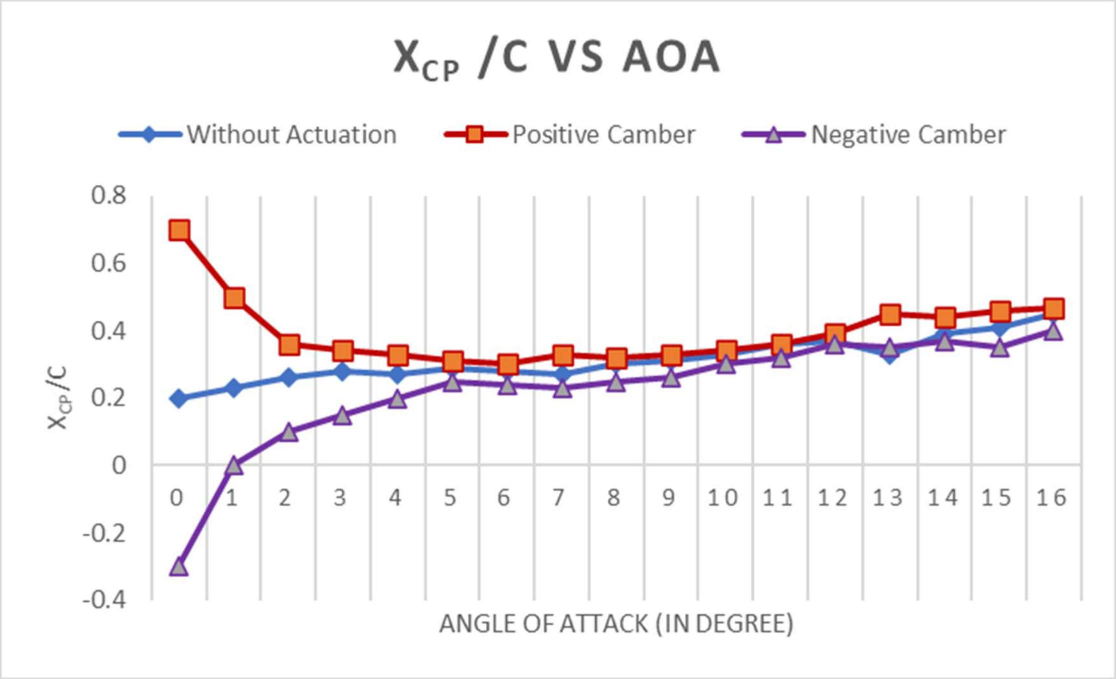

Fig 5.5 (l) X_{cp}/C vs Angle of Attack (α)

After the computational fluid dynamics (CFD) simulation was completed, the aerodynamics data were noted and presented in the following figures after the computational fluid dynamics (CFD) simulation was completed to conduct comprehensive improved aerodynamics performance. We now know that we can expand (positive camber), squeeze (negative camber), or maintain the top and bottom surfaces of the aerofoil unchanged without utilizing external voltage or actuation by employing piezoelectric macro fiber composites (MFC) as an actuator. The velocity at which this computation investigation was performed was from 2 m/s to 35 m/s within this range.

From figure 5.5 (g), we get an idea of how the actuation comes into consideration for improving the lift coefficient (CL), which is very important in aircraft aerodynamics. From these three types of scenarios, we can see that when the positive camber is being applied, the MFC is used to expand the aerofoil, there is a lift coefficient, and hence, the slope of this curve improves.

Figure 5.5 (h) shows the drag coefficient (CD) versus angle of attack () plot. Negative camber produces the most drag. Here, we can see the benefits of using piezoelectric actuation or the positive camber, which help to reduce or obtain the minimum amount of drag. The ratio of lift and drag is known as aerodynamics efficiency, and it is vital in defining aircraft performance. From the lift to drag ratio plot in figure 5.5 (i), there is also noticeable a vast improvement in the lift to drag ratio vs angle of attack, and the effect of positive camber and actuation is massive. The final output is way larger (about 500%) than no actuation and negative camber aerofoil.

Because of the incorporation of piezoelectric actuation via MFC patches, the lift coefficient (CL) versus Drag Coefficient (CD) plot in figure 5.5(j) also shows a significant improvement. A pitching moment is less likely expected for a stable flight. Figure 5.5 (k) shows that for the same flying situation, positive actuation or camber generates the least amount of pitching moment compared to negative camber and no actuation, which is a significant benefit. Figure 5.5 (l) demonstrates that the position of the aircraft's center of pressure (Xcp) may be changed using piezoelectric actuation or modifying camber, allowing the aircraft's stability and center of pressure to be tailored without impacting its pitching moment [19].

CHAPTER 6

CONCLUSION AND FUTURE WORKS

6.1 Conclusion

Piezoelectric energy harvesting from vibration sources has been widespread in recent decades, and many studies have been conducted. However, piezoelectric energy harvester is usually in unimorph or biomorph configuration made of monolithic piezoceramic layers. Nevertheless, piezoceramic is very brittle and has a limited operation environment. Because MFC patches are flexible compared to the brittleness of monolithic piezoceramic layers, they are remarkably durable to use in a wide variety of operating settings.

In the recent work, computational fluid dynamics (CFD) and finite element analysis (FEA) software were used to verify some of the existing works performed in energy harvesting and wing morphing design. Using piezoelectric macro fiber composites (MFC) and new three types of substrates materials, copper, zinc alloy and galvanized steel were used along with MFC patches as a substrate to harvest energy from vibrating sources and excitation from an aerofoil. Based on the mathematical model established before and experimental flight test data received from a real-life wind tunnel experiment, computational analysis was done, and a comparative and extensive investigation was undertaken. Along with the previously utilized various substrates, these three new substrates material with macro fiber composites (MFC) patches is expected to enlarge the existing knowledge domain in this field. Peak power output and voltage output were measured for each substrate's material for three thicknesses. The best performing substrate material was identified among these three and the most suitable thickness. Then, a computational fluid domain was built based on the available experimental information to simulate real-world wind tunnel testing.

The highest performing substrate material created a thing aerofoil surface with an MFC patch connected to the top surface. The model was tested in various flow velocities and angle of attack configurations. The macro fiber composites (MFC) patches were used as a transducer, which means vibration was provided from external sources as an energy harvester. However, the MFC patches were used as an actuator for the next part of the study. Voltage was applied externally to change the shape of the aerofoil. NACA 0010 aerofoil was chosen for this part, and its top and bottom surface was remodeled using MFC patches. It was tested that when a precise external voltage is provided to extend the aerofoil surface outward, its camber increases. It took the shape of a NACA 0012 aerofoil, and the detailed CFD simulation for this modelled NACA 0012 aerofoil was conducted. A detailed study was performed for three different situations. No actuation was provided means no camber, and while negative camber was applied, the aerofoil surface was squeezed inward. Positive camber/actuation improves the aerodynamics performance and offers superior inflight operation and stability of the aircraft, according to all experimental and computational findings.

6.2 Future Works

This research utilizes three novel substrate materials for piezoelectric energy harvesting from macro fiber composites (MFC). This analysis and study relied entirely on a computational examination based on the most up-to-date experimental and mathematical models. However, detailed experimental analysis is still needed to verify the results that were out of this work's scope and remain unchecked for further investigation in the future.

The fundamental challenge with power/energy harvesting utilizing macro fiber composites was that it depended on the amount of strain caused by aerodynamics or structural loading on the aircraft/wing/aerofoil, which was usually relatively low and varied throughout the flight regime. The popularity of macro fiber composites in the research field was always esteemed. The main reason was its high efficiency to produce energy by utilizing low strain or externally applied load.

However, this produced energy is good enough for incorporating an inflight wireless structural health monitoring system for the next generation of aircraft. However, it is challenging for scientists and researchers regarding the harvested energy for inflight systems. For that case, innovation of more efficient piezo ceramic materials is a need that will produce enough power even though the strain due to loading is less and not constant through the whole flight time. Engineers may face additional issues in storing this captured energy since increasing the number of batteries might result in a significant weight penalty for aeronautical vehicles.

REFERENCES

[1] Sodano, H., Inman, D., Park, G. A Review of Power Harvesting from Vibration using Piezoelectric Materials, The Shock and Vibration Digest, Vol. 36, No. 3, 197–205 May 2004

[2] Schultz, M.R., Hyer, M.W. (2004), A Morphing Concept Based on Unsymmetric Composite Laminates and Piezoceramic MFC Actuators, 45th AIAA/ ASME/ ASCE/ AHS/ASC Structures, Strutural Dynamics &Materials Conference, , Palm Spring, California, 19-22 April 2004

[3] Lanza Discalea, F., Matt, H., Bartoli, I., Coccia, S., Park, G., & Farrar, C. Health monitoring of UAV wing skin-to-spar joints using guided waves and macro fiber composite transducers, Journal of intelligent material systems and structures, 18(4), 373-388, 2007

[4] Park, G., Rutherford, A. C., Wait, J. R., Nadler, B., Farrar, C., & Claytor, T. N. High-frequency response functions for composite plate monitoring with ultrasonic validation, AIAA journal, 43(11), 2431-2437, 2005.

[5] Thien, A. B., Chiamori, H. C., Ching, J. T., Wait, J. R., & Park, G., The use of macro-fiber composites for pipeline structural health assessment. Structural Control and Health Monitoring, The Official Journal of the International Association for Structural Control and Monitoring and of the European Association for the Control of Structures, 15(1), 43-63, 2008.

[6] Sodano, H. A., Inman, D. J., & Park, G., Comparison of piezoelectric energy harvesting devices for recharging batteries, Journal of intelligent material systems and structures, 16(10), 799-807, 2005.

[7] Arms, S. W., Townsend, C. P., Churchill, D. L., Augustin, M., Yeary, D., Darden, P., & Phan, N., Tracking pitch link dynamic loads with energy harvesting wireless sensors, In Annual Forum Proceedings-American Helicopter Society (Vol. 63, No. 2, p. 934). American Helicopter Society, Inc., May 2007

[8] Bilgen, O., Kochersberger, K., Diggs, E. C., Kurdila, A., J., Inman, D., J., Morphing Wing Aerodynamic Control via Macro-Fiber Composite Actuators in an Unmanned Aircraft, AIAA 2007 Conference and Exhibit, Rohnert Park, California, 7-10 May 2007

[9] Bilgen, O., Kochersberger, K., Diggs, E. C., Kurdila, A., J., Inman, D., J., Morphing Wing Micro-Air-Vehicles via Macro-Fiber-Composite Actuators, 48th AIAA/ ASME/ ASCE/ AHS/ASC Structures, Structural Dynamics & Materials Conference, Honolulu, Hawaii, 23-26 April 2007

[10] Nuffer, D. J., Schönecker, D., Kohlrautz, D., Michelis, D. P., Adarraga, O., & Wolf, D. K. , Reliability investigation of piezoelectric macro fiber composite (MFC) actuators, Adaptronic Cong, 2007

[11] Song, H. J., Choi, Y. T., Wereley, N. M., & Purekar, A. S., Analysis of energy harvesting devices using macro-fiber composite materials, In ASME 2007 International Design Engineering Technical Conferences and Computers and Information in Engineering Conference (pp. 289-298). American Society of Mechanical Engineers, January 2007

[12] Daue, T. P., Kunzmann, J., & Schoenecker, A., Energy harvesting systems using piezo-electric macro fiber composites, In IEEE International Symposium on Electrets (ISE13), paper (Vol. 27), 2008

[13] Erturk, A., Bilgen, O., Fontenille, M., & Inman, D. J., Piezoelectric energy harvesting from macro-fiber composites with an application to morphing wing aircrafts, In Proceedings of the 19th International Conference on Adaptive Structures and Technologies, Ascona, Switzerland, Oct (pp. 6-9), October 2008

[14] Anton, S. R., & Inman, D. J. ,Vibration energy harvesting for unmanned aerial vehicles, In Active and Passive Smart Structures and Integrated Systems (Vol. 6928, p. 692824), International Society for Optics and Photonics, April 2008

[15] Yang, Y., Tang, L., & Li, H. ,Vibration energy harvesting using macro-fiber composites. Smart materials and structures, 18(11), 115025, 2009

[16] Song, H. J., Choi, Y. T., Wereley, N. M., & Purekar, A. S., Energy harvesting devices using macro-fiber composite materials, Journal of Intelligent Material Systems and Structures, 21(6), 647-658, 2010

[17] Marco Debiasi ,Yann Bouremel, Khoo Hock Hee, Luo Siao Chung and Elvin Tan Zhiwei, Shape Change of the Upper Surface of an Airfoil by Macro Fiber Composite Actuators, 29th AIAA Applied Aerodynamics Conference, 27 - 30 June 2011

[18] Marco Debiasi ,Yann Bouremel, Khoo Hock Hee, Luo Siao Chung and Elvin Tan Zhiwei, Deformation of the Upper Surface of an Airfoil by Macro Fiber Composite Actuators, 30th AIAA Applied Aerodynamics Conference, New Orleans, Louisiana, 27 - 30 June 2011

[19] Marco Debiasi, Yann Bouremel, Zhenbo Lu, Varsha Ravichandran, Deformation of the Upper and Lower Surfaces of an Airfoil by Macro Fiber Composite Actuators, 31st AIAA Applied Aerodynamics Conference, San Diego, CA, June 24-27, 2013

[20] Thornburhg,R.P., Kreshock,A.,R., Wilbur,M.,L., Sekula, M.,K.,Shen,J., Continuous Trailing-Edge Flaps for Primary Flight Control of a Helicopter Main Rotor, AHS 70th Annual Forum, Montréal, Québec, Canada, May 20–22, 2014

[21] Kelvin P. Ofori-Atta, Morphing Wings Using Macro Fiber Composites, McNair Scholars Research Journal, Volume 1, Article 10, 2014

[22] Rosario, M., Binante, V., Botturi, S., Massai, A., On the active deformations of hybrid specimens, Aircraft Engineering and Aerospace Technology: An International Journal, Volume 88, Number 5 , 2016

[23] Thornburgh, R., P., Kreshock, A., R., Wilbur, M., L., Experimental Measurement of a Blade Section With a Continuous Trailing-Edge Flap, AHS 72nd Annual Forum, West Palm Beach, Florida, USA, May 17-19, 2016

[24] Grzybek, D., & Micek, P. , Experimental investigations on energy harvesting from mechanical vibrations of buildings using macro fiber composite, Mechanics and Control, 35(1), 2016

[25] Shi, Y., Hallett, S. R., & Zhu, M., Energy harvesting behavior for aircraft composites structures using macrofibre composite: Part I–Integration and experiment. Composite Structures, 160, 1279-1286, 2017

[26] Sun, W., Tan, T., Yan, Z., Zhao, D., Luo, X., & Huang, W., Energy harvesting from water flow in open channel with macro fiber composite, AIP Advances, 8(9), 095107, 2018

[27] Hamdan, A., Mustapha, F., & Sultan, M. T. H, The macrofibre composite–bonded effect analysis on the micro-energy harvester performance and structural health–monitoring system of woven kenaf turbine blade for vertical axis wind turbine application, Advances in Mechanical Engineering, 10(9), 1687814018802046, 2018

[28] Gao, F., Liu, G., Chung, B. L. H., Chan, H. H. T., & Liao, W. H., Macro fiber composite-based energy harvester for human knee, Applied Physics Letters, 115(3), 033901, 2019

[29]Cadogan, D., Smith, T., Uhelsky, F., MacKusick, M., "Morphing Inflatable Wing Development for Compact Package Unmanned Aerial Vehicles," AIAA Paper 2004- 1807, 45th AIAA/ASME/ASCE/AHS/ASC Structures, Structural Dynamics & Materials Conference, Palm Springs, California, April 2004.

[30] Debiasi, M., Bouremel, Y., Khoo, H. H., Luo, S. C., and Tan, E. Z., "Shape Change of the Upper Surface of an Airfoil by Macro Fiber Composite Actuators", AIAA Paper 2011- 3809, 29th AIAA Applied Aerodynamics Conference, Honolulu, HI, June 2011.

[31] Debiasi, M., Bouremel, Y., Khoo, H. H., Luo, S. C., "Deformation of the Upper Surface of an Airfoil by Macro Fiber Composite Actuators", AIAA Paper 2012-3206, 30th AIAA Applied Aerodynamics Conference, New Orleans, Louisiana, June 2012.

[32] Online link: https://www.electronicdesign.com/power/whatpiezoelectric-effect

[33] Flynn, A. M. and Sanders, S. R., "Fundamental limits on energy transfer and circuit considerations for piezoelectric transformers," IEEE Transaction on Power Electronics, Vol. 17, No. 1, pp. 8-14, 2002.

[34] Elvin, N. G., Elvin, A. A. and Spector, M., "A self-powered mechanical strain energy sensor," Smart Materials and Structures, Vol. 10, No. 2, pp. 293-299, 2001.

[35] Roundy, S., Wright, P. K. and Rabaey, J., "A study of low level vibrations as a power source for wireless sensor nodes," Computer Communications, Vol. 26, pp. 1131-1144, 2003.

[36] Roundy, S. and Wright, P. K., "A piezoelectric vibration based generator for wireless electronics," Smart Materials and Structures, Vol. 13, No. 5, pp. 1131-1142, 2004.

[37] Roundy, S., Leland, E. S., Baker, J., Carleton, E., Reilly, E., Lai, E., Otis, B., Rabaey, J. M., Wright, P. K. and Sundararajan, V., "Improving power output for vibrationbased energy scavengers," IEEE Pervasive Computing, Vol. 4, No. 1, pp. 28-36, 2005.

[38] Leland, E. S. and Wright, P. K., "Resonance tuning of piezoelectric vibration energy scavenging generators using compressive axial preload," Smart Materials and Structures, Vol. 15, No. 5, pp. 1413-1420, 2006.

[39] Sodano, H. A., Park, G. H., Leo, D. J. and Inman, D. J., "Electric power harvesting using piezoelectric materials," Center for Intelligent Material Systems and Structures, Virginia Polytechnic Institute and State University, 2003.

[40] Sodano, H. A., Inman, D. J. and Park, G. H., "Comparison of piezoelectric energy harvesting devices for recharging batteries," Journal of Intelligent Material Systems and Structures, Vol. 16, No. 10, pp. 799-807, 2005.

[41] Shen, D., Park, J. H., Noh, J. H., Choe, S. Y., Kim, S. H., Wikle, H. C. and Kim, D. J., "Micromachined PZT cantilever based on SOI structure for low frequency vibration energy harvesting," Sensors and Actuators A: Physical, Vol. 154, No. 1, pp. 103-108, 2009.

[42] Liu, J., Fang, H., Xu, Z., Mao, X., Shen, X., Chen, D., Liao, H. and Cai, B., "A MEMS-based piezoelectric power generator array for vibration energy harvesting," Microelectronics Journal, Vol. 39, No. 5, pp. 802-806, 2008.

[43] Choi, W. J., Jeon, Y., Jeong, J. H., Sood, R. and Kim, S. G., "Energy harvesting MEMS device based on thin film piezoelectric Cantilevers," Journal of Electroceramics, Vol. 17, No. 2-4, pp. 543-548, 2006.

[44] Kim, H. W., Priya, S., Uchino, K. and Newnham, R. E., "Piezoelectric energy harvesting under high pre-stressed cyclic Vibrations," Journal of Electroceramics, Vol. 15, No. 1, pp. 27-34, 2005.

[45] Li, X., Guo, M. and Dong, S., "A flex-compressive-mode piezoelectric transducer for mechanical vibration/strain energy harvesting," IEEE Transactions on Ultrasonics, Ferroelectrics and Frequency Control, Vol. 58, No. 4, pp. 698-703, 2011.

[46] Adhikari, S., Friswell, M. I. and Inman, D. J., “Piezoelectric energy harvesting from broadband random vibrations,” Smart Materials and Structures, Vol. 18, No. 11, Paper No. 115005, 2009.

[47] Lefeuvre, E., Badel, A., Richard, C., Petit, L. and Guyomar, D., “A comparison between several vibration-powered piezoelectric generators for standalone systems,” Sensors and Actuators A: Physical, Vol. 126, No. 2, pp. 405-416, 2006.

[48] Yoon, H. S., Washington, G. and Danak, A., “Modeling, optimization, and design of efficient initially curved piezoceramic unimorphs for energy harvesting applications,” Journal of Intelligent Material Systems and Structures, Vol. 16, No. 10, pp. 877-888, 2005.

[49] Yoon, S. H., Lee, Y. H., Lee, S. W. and Lee, C., “Energyharvesting characteristics of PZT-5A under gunfire shock,” Materials Letters, Vol. 62, No. 21-22, pp. 3632-3635, 2008.

[50] Chen, Z. G., Hu, Y. T. and Yang, J. S., “Piezoelectric generator based on torsional modes for power harvesting from angular vibrations,” Applied Mathematics and Mechanics, Vol. 28, No. 6, pp. 779-784, 2007.

[51] Erturk, A. and Inman, D. J., “Issues in mathematical modeling of piezoelectric energy harvesters,” Smart Materials and Structures, Vol. 17, No. 6, Paper No. 065016, 2008.

[52] Erturk, A. and Inman, D. J., “On Mechanical modeling of cantilevered piezoelectric vibration energy harvesters,” Journal of Intelligent Material Systems and Structures, Vol. 19, No. 11, pp. 1311-1325, 2008.

[53] Erturk, A. and Inman, D. J., “An experimentally validated bimorph cantilever model for piezoelectric energy harvesting from base excitations,” Smart Materials and Structures, Vol. 18, No. 2, Paper No. 025009, 2009.

[54] Marqui Junior, C. D., Erturk, A. and Inman, D. J., “An electromechanical finite element model for piezoelectric energy harvester plates,” Journal of Sound and Vibration, Vol. 327, No. 1-2, pp. 9-25, 2009.

[55] Renno, J. M., Daqaq, M. F. and Inman, D. J., “On the optimal energy harvesting from a vibration source,” Journal of Sound and Vibration, Vol. 320, No. 1-2, pp. 386-405, 2009.

[56] Poulin, G., Sarraute, E. and Costa, F., “Generation of electrical energy for portable devices comparative study of an electromagnetic and a piezoelectric system,” Sensors and Actuators A: Physical, Vol. 116, No. 3, pp. 461-471, 2004.

[57] Ajitsaria, J., Choe, S. Y., Shen, D. and Kim, D. J., “Modeling and analysis of a bimorph piezoelectric cantilever beam for voltage generation,” Smart Materials and Structures, Vol. 16, No. 2, pp. 447-454, 2007.

[58] Hu, Y. T., Hu, T. and Jiang, Q., “Coupled analysis for the harvesting Structure and the modulating circuit in a piezoelectric bimorph energy harvester,” Acta Mechanica Solida Sinica, Vol. 20, No. 4, pp. 296-308, 2007.

[59] Shu, Y. C. and Lien, I. C., “Efficiency of energy conversion for a piezoelectric power harvesting system,” Journal of Micromechanics and MicroEngineering, Vol. 16, No. 11, pp. 2429-2438, 2006.

[60] Marzencki, M., Defosseux, M. and Basrour, S., “MEMS vibration energy harvesting devices with passive resonance frequency adaptation capability,” Journal of Microelectromechanical Systems, Vol. 18, No. 6, pp. 1444- 1453, 2009.

[61] Erturk A and Inman D J 2008 A distributed parameter electromechanical model for cantilevered piezoelectric energy harvesters ASME Journal of Vibration and Acoustics 130:041002

[62] Erturk A and Inman D J 2009 An experimentally validated bimorph cantilever model for piezoelectric energy harvesting from base excitations Smart Materials and Structures accepted

[63] IEEE Standard on Piezoelectricity 1988 IEEE, New York.

[64] Ming Yuan, Ziping Cao, Jun Luo, Characterization the influences of diodes to piezoelectric energy harvester, International Journal of Smart and Nano Materials 9(3):1-16, March 2018

[65] M.Bhanusri, Design and simulation of piezoelectric energy harvesting system (file:///C:/Users/saifu/Desktop/Masters%20Degree/bhanusri_paper.pdf)

[66] E.varadrajan,M.Bhanusri, Design and Simulation of Unimorph Piezoelectric Energy Harvesting System (file:///C:/Users/saifu/Desktop/Masters%20Degree/bhanusri_paper.pdf)

[67] Roundy, S., Wright, P.K and Rabaey, J., “A study of low-level vibrations as a power source for wireless nodes,” Computer Communications, Vol.26, pp.1131-1144,2003